Journal of Neuroinflammation

RESEARCH

Open Access

TRPM7 contributes to pyroptosis and its involvement in status epilepticus

Xin Tong[1,2†], Yu Tong[2†], Jiahe Zheng[3†], Ruixue Shi[2†], Hongyue Liang[2], Meixuan Li[2], Yulu Meng[2], Jian Shi[2], Dongyi Zhao[2], Corey Ray Seehus[4], Jialu Wang[5], Xiaoxue Xu[5], Tomasz Boczek[6], Sayuri Suzuki[7,8], Andrea Fleig[7,8,9], Reinhold Penner[7,8,9], Naining Zhang[10], Jianjun Xu[11], Jingjing Duan[12], Zhiyi Yu[10*], Wuyang Wang[13*], Weidong Zhao[14,15*] and Feng Guo[1,2*]

Abstract

Background Pyroptosis, a novel form of programmed cell death, has been implicated in neurodegeneration diseases. However, its role in status epilepticus (SE)—a condition characterized by prolonged or repeated seizures—remains inadequately understood.

Methods SE were induced by intraperitoneal injection of pilocarpine (PILO). Neuronal excitability was assessed through electroencephalogram (EEG) recordings and patch clamp. Chromatin immunoprecipitation (ChIP) assay was applied to verify the interaction of phosphorylated signal transducer and activator of transcription 3 (p-STAT3) protein with the promoters of *Nlrp3* (the gene encoding NOD-like receptor family pyrin domain containing 3) and *Trpm7* (transient receptor potential melastatin 7). To further investigate the role of TRPM7 in SE, AAV-sh-TRPM7-EGFP transfected mice and TRPM7 conditional knockout (TRPM7-CKO) mice were utilized.

Results Our findings revealed elevated levels of IL-18 and IL-1β levels in primary epilepsy patients, along with increased expression level of the TRPM7 in SE models. Knockdown of TRPM7 alleviated neuronal damage and pyroptosis, reversing PILO-treated neuronal hyperexcitability. We demonstrated that p-STAT3 binds to the promoters of both *Trpm7* and *Nlrp3*, modulating their transcriptions in SE. Importantly, inhibition of TRPM7 with NS8593, and inflammasome inhibition with MCC950, alleviated neuronal hyperexcitability and pyroptosis in SE. A new compound, SDUY-225, formulated based on the structure of NS8593 mitigated neuronal damage, pyroptosis, and hyperexcitability.

Conclusions TRPM7 contributes to pyroptosis in SE, establishing a positive feedback loop involving the p-STAT3/TRPM7/Zn^{2+}/p-STAT3 signaling pathway. Findings in this study raise the possibility that targeting TRPM7 and NLRP3 represents a promising therapeutic approach for SE.

Keywords NLRP3, Pyroptosis, SE, STAT3, TRPM7, Zn^{2+}

†Xin Tong, Yu Tong, Jiahe Zheng, Ruixue Shi contributed equally to this work.

*Correspondence:
Zhiyi Yu
zhiyi_yu@sdu.edu.cn
Wuyang Wang
wuyangwang80@gmail.com
Weidong Zhao
wdzhao@cmu.edu.cn
Feng Guo
blueforest611@hotmail.com
Full list of author information is available at the end of the article

Introduction

Pyroptosis is a newly recognized form of programmed cell death, mediated by gasdermin D (GSDMD), which leads to the activation of proinflammatory cytokines like IL-18 and IL-1β [1]. Pyroptosis has been associated with the pathogenesis of innate immunity and diseases [2], which has been implicated in neurodegenerative disorders including atherosclerosis, Parkinson's disease (PD), Alzheimer disease (AD), etc [1, 3].

Epilepsy, a common neurological disease affecting more than 70 million people worldwide, results from abnormal neuronal discharges of neurons and is featured in recurrent, and unpredictable seizures [4]. Status epilepticus (SE) is a particularly severe form of episode, defined as a continuous seizure lasting over 5 min or a series of seizures occurring within a 30 min period without a return to baseline [5]. The administration of pilocarpine (PILO) and Mg^{2+}-free extracellular fluid could give rise to SE, which has been widely used in previous studies [6, 7]. Recent research has linked pyroptosis to SE, with studies demonstrating elevated levels of NOD-like receptor family, pyrin domain containing 3 (NLRP3), caspase-1, GSDMD, IL-18, and IL-1β in epilepsy animal models [8–12]. Inhibiting components of the NLRP3 inflammasome, such as NLRP3 or caspase-1, has been shown to curtail hippocampal neuronal loss and deters the development of spontaneous recurrent seizures [10]. It's noteworthy that patients with epilepsy have been found to express higher levels of NLRP1 and NLRP3 in the hippocampus,[13] although the intricate mechanisms by which pyroptosis contribute to SE remains unclear.

The melastatin-related transient receptor potential (TRPM) subfamily is a membrane protein and play pivotal roles in a myriad of physiological and pathophysiological processes [14]. The TPRM subfamily branches further into TRPM1-TRPM8, each permitting different ions to pass through their channel pores [15]. Among them, TRPM7 is highly expressed in the brain and has been associated with several neurological disorders including brain ischemia, Parkinson's disease, and amyotrophic lateral sclerosis, but its participation in epilepsy is rarely investigated [16–19]. TRPM7 is a divalent cation channel permeable to Ca^{2+}, Mg^{2+}, Mn^{2+}, and, notably Zn^{2+}.[20] Additionally, while carvacrol and 2-APB (TRPM7 inhibitors), reversed neuronal death by reducing Zn^{2+} accumulation [21]. However, the role of TRPM7-mediated Zn^{2+} in SE and its potential involvement in pyroptosis has not been demonstrated.

Here, for the first time, our work clarified the detailed mechanism on how TRPM7 participates in pyroptosis and epileptogenesis, and how targeting TRPM7 may pave the way for a new generation of drugs to treat SE and other neurological conditions, among which neuronal pyroptosis is a hallmark pathology.

Materials and methods

The detailed procedures were showed in supplementary file.

Animals and drug administration

All the animals were raised in a standard environment with controlled temperature on a 12 h light/dark cycle, and maintained in the Institutional Animal Care and Use Committee of China Medical University. An equal number of male and female mice 8–12 weeks old were used for each experiment. Status epilepticus (SE) was induced by pilocarpine (PILO, 300 mg/kg i.p.) [22, 23]. Mice that experienced seizures (scores IV and V on the Racine scale) were used in subsequent experiments. All animal protocols were approved by the Institutional Animal Care and Use Committee of China Medical University.

Cell culture and drug administration

The mouse neuroblastoma neuro-2a (N2a) cells were purchased from Fenghbio. The murine microglial cell line BV2 cells were purchased from Procell Co., Ltd. All cell lines were cultured in 10% FBS DMEM with 1% penicillin–streptomycin antibiotic mixture medium.

Cell viability assay

The cell viability was measured by the Cell Counting Kit-8 assay (CCK-8, Abbkine, BMU106-CN). The N2a cells were seeded in 96-well plates and treated with a range of concentrations of PILO including 2, 4, 8, 16, 32, 64, 128, and 256 mM for 48 h, and then analyzed the cell viability according to the manufacturer' s instructions.

Small interfering RNA (siRNA) and overexpression plasmid transfection

Knockdown of TRPM7 was conducted by using specific siRNA synthesized by GenePharm, and the siRNA against signal transducer and activator of transcription 3 (STAT3) was obtained from JTS scientific. TRPM7 (ion channel segment) overexpression plasmid was a gift from Professor Jingjing Duan' s lab in Nanchang university in China. The siRNA and DNA plasmids were transfected with the Lipo8000™ transfection reagent (Beyotime) according to the manufacturer's instructions. All overexpression and siRNA target sequences were provided in Supplemental Table 1.

Real-time qRT-PCR

Total RNA was extracted and purified with the RNAiso Plus (TaKaRa). For real-time quantitative reverse transcription PCR (qRT-PCR), the 2×SYBR Green qPCR

Master Mix (Bimake) was used and the samples were amplified via the QuantStudio1 (Applied Biosystems). All primers used were listed in Supplemental Table 2.

Chromatin immunoprecipitation (ChIP) assay

After 24 h pretreatment with or without PILO (12 mM), N2a cells were harvested for ChIP. Chromatin was crosslinked for 10 min at 37 °C with 1% formaldehyde directly added to cell culture medium, followed by sonicated, diluted, and immunoprecipitated with anti-STAT3 (CST, #12,640), anti- phospho-STAT3 (CST, #9145) or normal mouse IgG (Santa Cruz, sc-2025) antibody at 4 °C overnight. Protein A-Sepharose beads were added and then washed successively with low-salt buffer, high-salt buffer, LiCl buffer, and TE buffer. The protein-DNA complexes were eluted and the crosslinking was reversed at 65 °C. DNA fragments were purified and analyzed by qRT-PCR. The primers used in qRT-PCR were listed in Supplemental Table 3.

Primary neuron cultures

Primary neuron cultures were prepared as described previously [24, 25]. Hippocampal neurons were obtained from Wistar rat embryonic brains and plated on 6 well glass bottom plates coated with 0.01% poly-L-Lysine (Sigma-Aldrich) and 0.1 mg/mL laminin (ThermoFisher Scientific). On day 7–9, hippocampal neurons were prepared for drug administrations.

Chemical synthesis

All reagents and solvents were purchased from commercial sources and used without further purification. Reactions were monitored by thin-layer chromatography (TLC) on 0.25 mm silica gel plates, and the spots were visualized with UV light, and iodine vapor. Mass spectra were obtained using ESI–MS spectrometry instrument model API4000 manufactured by Thermo Fisher.

Patch clamp

Action potential studies were performed in the whole-cell current-clamp mode. The extracellular bath solution containing (in mM): 145 NaCl, 4 KCl, 1 $MgCl_2$, 1.8 $CaCl_2$, 10 HEPES, and 10 Glucose; pH 7.35 (~310 mOsm). The pipettes solution containing (in mM): 140 K-gluconate, 3 KCl, 10 HEPES, 0.2 EGTA, 2 $MgCl_2$, and 2 Na_2ATP_3; pH 7.25 (280–290 mOsm). Electrophysiological recordings were conducted and partially modified based on the previous study [26]. Action potentials were evoked by a 1-s depolarizing current injection with a maximum of 200 pA in a ramp mode. Membrane potential was clamped to − 80 mV for both spontaneous and evoked action potential firing measurements. Patch clamping was carried out using an EPC-10 amplifier and a PatchMaster software (HEKA, Lambrecht, Germany). All experiments were carried out at room temperature (22 ± 2 °C), and data were analyzed via Igor Pro 6.12A software.

Stereotaxic injection

Mice were anesthetized with isoflurane, and then fixed into a stereotaxic instrument (ZS-FD Zhongshi Dichuan). A total volume of 1μL virus: (a) Recombinant TRPM7 knockdown adeno-associated virus (pAAV-U6-shRNA (Trpm7)-CMV-EGFP-WPRE) with titer 7.39E + 12 vg/mL, (b) NC (pAAV-U6-shRNA (NC2)-CMV-EGFP-WPRE-spolyA) with titer 1.18E + 13 vg/mL, obtained from OBIO Technology, were injected into the location within the ventral hippocampus (AP: − 3.28 mm, ML: ± 2.75 mm, DV: − 2.5 mm) [27]. Stereotaxic injection was operated with syringe pump R462 (RWD Life Science Co., Ltd). 1μL of virus was injected at each DV location in 1μL increments at a ow rate of 1μL /min.

Electroencephalogram (EEG) recordings

Both stainless steel screws (1.0 mm diameter) and single tungsten LFP electrodes (0.08 mm diameter, 1.5mm length) serving as EEG electrodes were placed over the bilateral somatosensory cortex (AP: − 1.0 mm, ML: ± 1.5 mm) under 1–1.5% isoflurane anesthesia [28]. A reference screw electrode was implanted on the cerebellum. EEG electrodes were attached to a head device (Bio-Signal Technologies, 2625) by silver wires (100 μm), then the assembly was secured with dental cement. One week after mice surgery, cortical EEG signals were amplified, filtered, and digitalized with a resolution of 1000 Hz using a tethered data acquisition system (Bio-Signal Technologies) and continuously synchronized with infrared video for at least one hour and then analyzed off-line in the custom code and brainstorm based on Matlab 2021.

Zn^{2+} staining

Under the light proof condition, the 20 μm brain slices were immersed in a solution of 4.5 μM TSQ (AAT BIOQUEST, 21,254), 140 mM sodium barbital, and 140 mM sodium acetate (pH 10.5–11) for five minutes and then rinsed twice with PBS. The coronal sections from each animal were observed and photographed under fluorescent microscopy (Olympus BX61) with 360 nm UV light. The mean gray value of TSQ-stained area was expressed using ImageJ software.

Immunofluorescence

The hippocampal neurons were seeded on cell climbing sheets. Brains of mice were embedded in optimum cutting temperature compound (OCT, SAKURA) and coronally sectioned with a 20 μm thickness. Neurons

and sections were fixed by 4% PFA for 10 min and then permeated membrane using 0.3% Triton X-100 (Solarbio, Beijing, China) for 10 min at room temperature before blocked (at room temperature for 1 h) using 5% BSA blocking buffer (Solarbio). Next, the neurons were incubated at 4 ℃ for 1 h with primary antibodies. And the sections were incubated overnight at 4 ℃ with primary antibodies. The following primary antibodies were used at 1:100: anti-TRPM7 (Abcam, ab729), anti-NLRP3 (Proteintech, 19771–1-AP), anti-NeuN (Abcam, ab104224), and anti-GFAP (Bioawamp, PAB32097). Then neurons and sections were incubated with secondary antibody at room temperature for 2 h. Finally, the nuclei were stained with DAPI (Solarbio, C0060). Samples were observed and photographed under confocal fluorescence microscopy (Nikon A1R).

Measurement of intracellular reactive oxygen species (ROS)

Intracellular ROS production was measured by using the reactive oxygen species assay kit (Beyotime) according to the manufacturer' s instructions. DCF fluorescence signals were determined by confocal fluorescence microscopy (Nikon A1R). Relative ROS was quantified from mean intensity of DCF fluorescence and normalized to control conditions.

Measurement of mitochondrial membrane potential (MMP)

The inner membrane electrical potential across mitochondrial membrane (MMP) in N2a cells was measured using JC-1 dye (Beyotime) according to the manufacturer' s instructions. JC-1 fluorescence signals were captured and recorded using confocal fluorescence microscopy (Nikon A1R). MMP fluorescence intensity was calculated as the red/green fluorescence ratio.

Western blot

The cytoplasmic and nuclear protein fractions were isolated using nuclear and cytoplasmic protein extraction kit (Beyotime Institute of Biotechnology, Haimen, China). 30 μg protein were separated by 12% SDS-PAGE and transferred to polyvinylidene fluoride membrane. Then the membranes were blocked and incubated with primary antibodies. The following primary antibodies were used at 1:1,000: anti-NLRP3 (ABclonal, A5652); anti-phospho-STAT3 (Tyr705) (Bioss, bs-1658R); anti-caspase 1 (Proteintech, 22915–1-AP); anti-GFAP (Bioawamp, PAB32097); anti-NeuN (Abcam, ab104224); anti-STAT3 (Proteintech, 10253–2-AP); anti-GSDMD (Abcam, ab219800); anti-phospho-JAK2 (Y1007 + Y1008) (Bioawamp, PAB30711); anti-JAK2 (Abcam, ab32101); and anti-Tubulin (Santa Cruz, sc-8035). The following primary antibodies were used at 1:5,000: anti-beta actin (Proteintech, 20536–1-AP); anti-TRPM7 (Abcam, ab245408); and anti-GAPDH (Proteintech, 10494–1-AP). The membranes were then incubated with HRP-labeled anti-rabbit, anti-mouse, or anti-goat (Proteintech) secondary antibodies.

Enzyme-linked immunosorbent assay (ELISA)

Human inflammatory cytokines (IL-1β and IL-18) were measured using ELISA kits (Wuhan ColorfulGene Biological Technology) as instructed by the manufacturer. The supernatants of hippocampus tissue, BV2 cells and N2a cells were harvested and measured for IL-1β and IL-18 release using ELISA kits (Bioswamp) following the manufacturer' s instructions. The human study complied with the Declaration of Helsinki and the ethical principles of the National Institutes of Health and was approved by the Committee on Human Research of the First Affiliated Hospital of China Medical University.

Patient samples

All human serum samples were obtained from the First Affiliated Hospital of China Medical University. Serum samples were obtained from 11 patients who diagnosed as idiopathic epilepsy and 9 healthy volunteers recruited from advertisements as the control group. Detailed information on the patients and volunteers were shown in Supplemental Table 4 and Table 5, respectively.

Statistics

All statistical analyses were performed by GraphPad Prism 9.0 software. Data were presented as mean ± SEM. P values < 0.05 were regarded statistically significant. Normal distribution and homogeneity of variances were evaluated using the Shapiro–Wilk test and Brown-Forsythe test, respectively. For normally distributed data, Student's t-test (± Welch correction) or one-way analysis of variance (ANOVA) was performed to determine significance. When there were two groups and one or more normality are rejected, Mann Whitney U test was performed. For three or more groups, when the main issue was whether a significant difference between groups and whether there are interactions between factors, one-way ANOVA or Kruskal Wallis ANOVA was performed depending on normality. When the ANOVA result was significant different ($P < 0.05$), the Tukey's multiple comparisons test was used.

Results

Pyroptosis was involved in SE but not in absence seizures

Pilocarpine (PILO) is a widely-used drug that induces spontaneous seizures and partially mimics temporal lobe epilepsy [7]. Here, we injected PILO to C57BL/6 J mice

to establish an in vivo model of status epilepticus (SE), according to the previous study [29].

We first conducted RNA sequencing on hippocampus from PILO-treated and vehicle-treated C57BL/6 J mice. In Fig. 1A, we identified 165 differentially expressed genes (DEGs) between PILO-treated mice and control mice, with 153 up-regulated genes and 12 down-regulated genes. Gene Ontology (GO) enrichment analysis (Fig. 1B) of the upregulated genes suggested that cell death processes were significantly activated in the PILO-induced SE model, potentially initiating epileptogenesis.

Pyroptosis is a programmed cell death that has been not commonly associated with the occurrence of SE, we then investigated whether pyroptosis associated factors were altered in patients with idiopathic epilepsy and the PILO-treated SE models. Serum levels of free IL-18 and IL-1β were significantly higher in idiopathic epilepsy

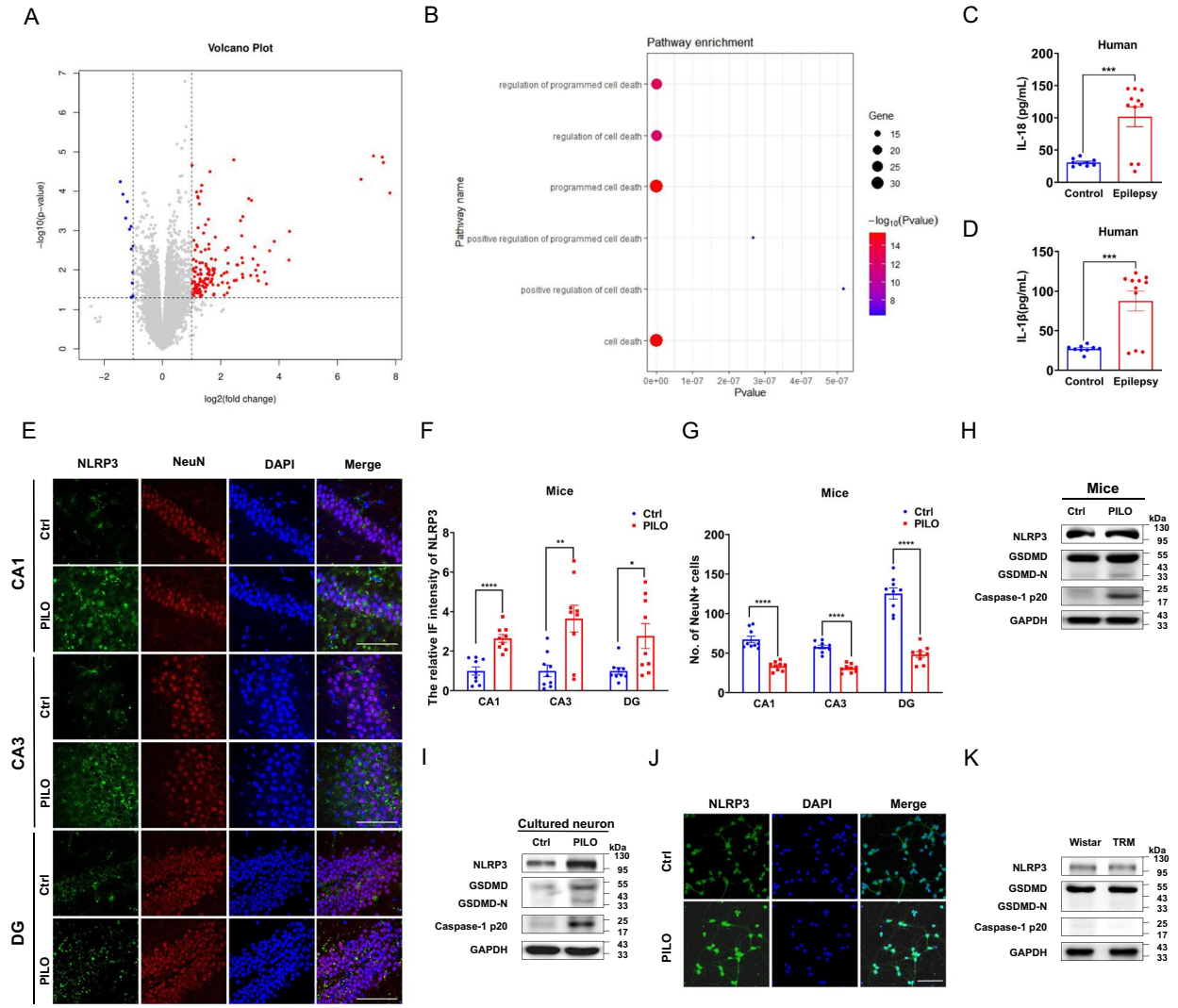

Fig. 1 Pyroptosis was involved in SE but not in absence seizures **A, B** The volcano plot and GO enrichment analysis of the DEGs in mice treated with PILO compared with healthy C57BL/6 J controls ($n=5$). The red dots represent up-regulated genes, while the blue dots represent down-regulated ones. **C, D** ELISA analysis of IL-18 (C) and IL-1β (D) in the serum of idiopathic epilepsy patients ($n=11$) and healthy controls ($n=9$). **E–G** Immunofluorescence analysis of NLRP3 (green) and NeuN (red) expression in hippocampus of PILO-treated C57BL/6 J mice (60 × lens), including the CA1, CA3 and DG regions ($n=9$). Scale bar: 100 μm. DAPI (blue) was used to label nucleus. **H, I** The representative protein bands of NLRP3, GSDMD-N, and caspase-1 p20 in hippocampus of PILO-treated C57BL/6 J mice ($n=6$) and cultured neurons treated with PILO for 24 h ($n=6$). **J** Immunofluorescence analysis of NLRP3 (green) expression in cultured neurons (20 × lens) treated with PILO for 24 h ($n=6$). Scale bar: 100 μm. DAPI (blue) was used to label nucleus. **K** The representative protein bands of NLRP3, GSDMD, and caspase-1 p20 of control Wistar and TRM rats ($n=6$). Full scans of all the blots are in the Supplementary Note. *$P<0.05$; ** $P<0.01$; *** $P<0.001$; **** $P<0.0001$

patients compared to healthy controls, as measured by ELISA (Fig. 1, C and D).

Additionally, the protein expression levels of NLRP3, GSDMD, and caspase-1 p20 (Fig. 1H) were enhanced in hippocampal tissues of PILO-treated SE mice, as confirmed by western blot. Moreover, we detected the expression of NLRP3 and neuronal nuclei (NeuN), a neuron marker, in hippocampus of PILO-treated SE mice by immunofluorescence. PILO-treated epileptic mice exhibited higher relative fluorescence intensity of NLRP3 in cornu ammonis 1 (CA1), cornu ammonis 3 (CA3), and dentate gyrus (DG) regions (Fig. 1, E and F). Meanwhile, the number of neurons were decreased in CA1, CA3, and DG regions (Fig. 1, E and G) of PILO induced SE mice.

Then, hippocampal neurons treated with 10 μM PILO for 24 h showed significantly increased protein levels of NLRP3, GSDMD, and caspase-1 p20 (Fig. 1I). For investigate the location and expression level of NLRP3 protein, immunofluorescence staining was performed in cultured hippocampal neurons after 10 μM PILO treatment for 24 h. 10 μM PILO treatment significantly enhanced the relative fluorescence intensity of NLRP3 (Fig. 1J).

The tremor rat (TRM) is capable to mimic human absence-like seizures and demonstrate spontaneous spike and wave discharges in electroencephalogram (EEG) recordings [30]. However, compared with the Wistar controls, the changes of pyroptosis associated factors including NLRP3, GSDMD, and caspase-1 p20 were unaltered (Fig. 1K) in TRM group, suggesting that pyroptosis was involved in SE but not in absence seizures.

To further explore the effects of PILO, we treated N2a cells with various concentrations of PILO and analyzed cell viability after 48 h using the CCK-8 assay. Cell vitality decreased in a dose-dependent manner, with a half maximal inhibitory concentration (IC_{50}) of 12 mM in N2a cells (Supplemental Fig. 1A). After treating N2a cells with 12 mM PILO for different time intervals 0 h, 12 h, 24 h, 36 h, and 48 h, we tested the changes of pyroptosis associated factors by western blot. Compared with the response at 0 h, protein levels of NLRP3, GSDMD, and caspase-1 p20 (Supplemental Fig. 1B) in 24 h group were significantly enhanced. As a positive control for caspase-1-dependent pyroptosis [31], N2a cells were pretreated with 1 μg/mL lipopolysaccharide (LPS) for 4 h and then were treated with 15 μM Nigericin for 1 h to measure the changes of pyroptosis associated factors. Compared with the control group, the protein levels of NLRP3, GSDMD, caspase-1 p20 (Supplemental Fig. 1C), IL-18 (Supplemental Fig. 1D), and IL-1β (Supplemental Fig. 1E) were significantly increased in the N2a cells of LPS group. Meanwhile, compared with the control group, the protein levels of pyroptosis associated factors (Supplemental Fig. 1, F–H) in the C57BL/6 J mice injected intraperitoneally with LPS (20 mg/kg) were also significantly increased. Taken together, PILO treatment can promote pyroptosis in SE models. Thus, pyroptosis was involved in SE but not in absence seizures.

TRPM7 was increased in SE models and participated in pyroptosis in vitro

TRPM7 has been involved in several neurological diseases including ischemic injury, Alzheimer's disease, and Parkinson's disease [32]. However, the relationship between TRPM7 and SE is currently unknown. We analyzed six transcriptome datasets of the hippocampus of normal mice (Supplemental Fig. 2A) and normal human (Supplemental Fig. 2B) brains, and found that TRPM7 was in the top three levels of TRPM subfamily gene expression in both healthy human and healthy mice hippocampal samples in each dataset. To investigate the involvement of TRPM7 in SE, we detected the change of TRPM7 in SE models in vivo and in vitro. TRPM7 protein expression in C57BL/6 J mice hippocampal tissues was enhanced in PILO-treated SE mice by western blot (Fig. 2, A, B). Moreover, we detected TRPM7 protein expression and the colocalization with NeuN in hippocampus of PILO-treated SE mice by immunofluorescence. The expression of TRPM7 was increased in CA1, CA3, and DG regions (Fig. 2, E and F) of PILO-treated SE mice. Additionally, PILO-treated SE mice exhibited higher amount of $TRPM7^+$ cells in $NeuN^+$ neurons in CA1, CA3, and DG regions (Fig. 2, E and G). Similarly, TRPM7 protein expression in Mg^{2+}-free treatment group (Fig. 2, C and D) was also increased. Consistently, PILO treatment significantly enhanced the expression of TRPM7 protein in PILO-treated hippocampal neurons (Fig. 2, C and D). Additionally, the protein expression of TRPM7 in PILO-treated N2a cells was significantly increased in PILO group compared with the control group (Fig. 2, H, I).

The relationship between TRPM7 and pyroptosis remained unclear and we hypothesized that TRPM7 could contribute to pyroptosis. Therefore, we transfected TRPM7 siRNA and TRPM7 (ion channel segment) overexpression plasmid into N2a cells to explore the relationship between TRPM7 and pyroptosis. The knockdown (Supplemental Fig. 2C) and overexpression (Supplemental Fig. 2D) efficiency were examined by real-time qRT-PCR. TRPM7 overexpression significantly enhanced the protein levels of NLRP3, GSDMD, and caspase 1 p20 (Fig. 2, J and K). Meanwhile, in empty vector-transfected N2a cells, PILO treatment elevated the protein levels of NLRP3, GSDMD, and caspase 1 p20 (Supplemental Fig. 2E). PILO treatment in TRPM7-overexpressed N2a cells further increased the protein levels of NLRP3, GSDMD, and caspase 1 p20 (Supplemental Fig. 2E).

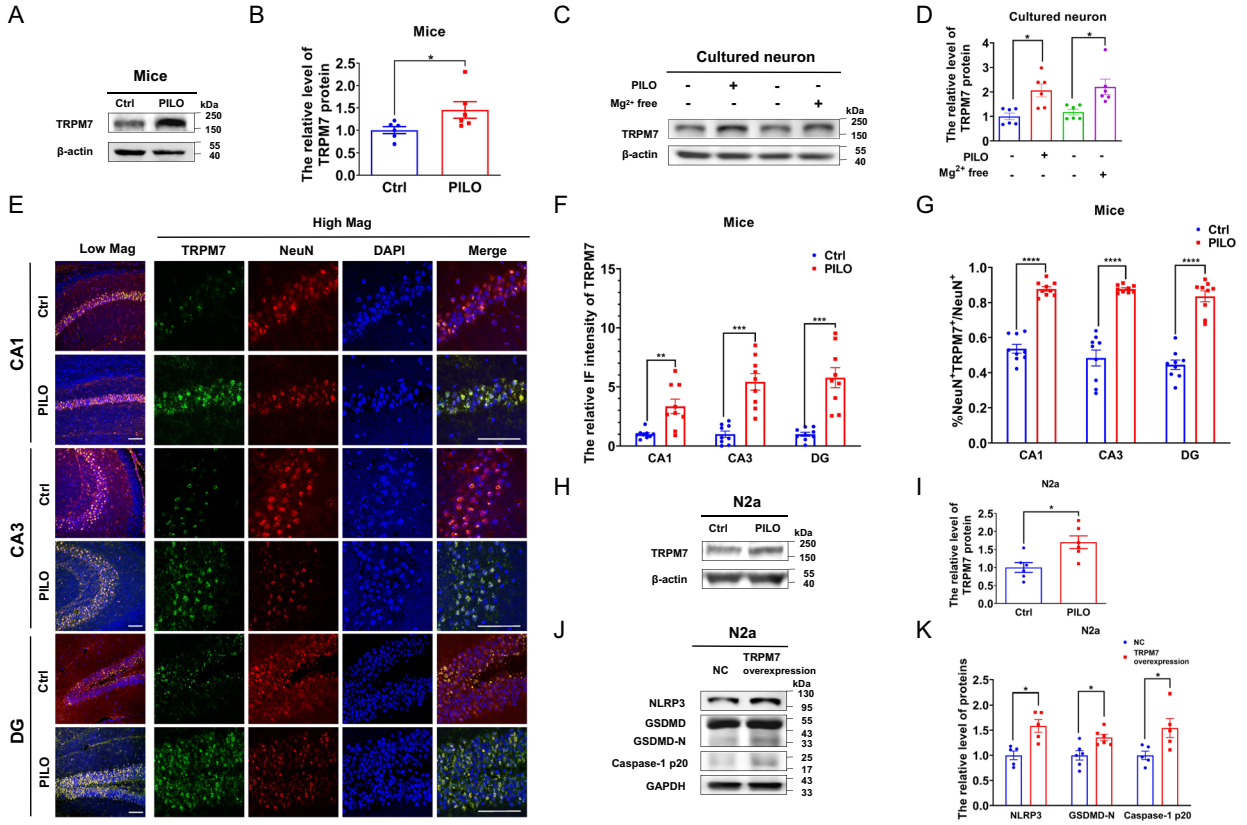

Fig. 2 TRPM7 was increased in SE models and participated in pyroptosis in vitro. **A**, **B** The representative protein bands and analysis of TRPM7 in hippocampus of PILO-treated C57BL/6 J mice ($n=6$). **C**, **D** The representative protein bands and analysis of TRPM7 of cultured neurons treated with PILO for 24 h or cultured in Mg^{2+}-free extracellular fluid for 3 h before cultured in the original medium for 21 h ($n=6$).**E–G** Immunofluorescence analysis of TRPM7 (green) and NeuN (red) expression in hippocampus of PILO-treated C57BL/6 J mice, including the CA1, CA3 and DG regions (20 × lens or 60 × lens). The arrows indicated positive co-localization neurons ($n=9$). Scale bar: 100 μm. DAPI (blue) was used to label nucleus. **H**, **I** The representative protein bands and analysis of TRPM7 in PILO-treated N2a cells ($n=6$). **J**, **K** The representative protein bands and analysis of NLRP3, GSDMD, and caspase-1 p20 in TRPM7-overexpressed N2a cells ($n=5$ or 6). Full scans of all the blots are in the Supplementary Note. *$P<0.05$; **$P<0.01$; ***$P<0.001$; ****$P<0.0001$

Additionally, PILO treatment significantly enhanced the protein levels of NLRP3, GSDMD, and caspase 1 p20 (Supplemental Fig. 2F). Following PILO treatment, the protein levels of NLRP3, GSDMD, and caspase 1 p20 (Supplemental Fig. 2F) were decreased in si-TRPM7-1 transfected N2a cells. In addition, the reduction in levels of NLRP3, GSDMD, and caspase 1 p20 (Supplemental Fig. 2F) protein were observed in si-TRPM7-2 transfected N2a cells.

Thus, TRPM7 was increased in SE models in vivo and in vitro and participated in pyroptosis.

TRPM7 contributed to pyroptosis in SE models in vivo

To further elucidate whether TRPM7 gene knockdown reduces pyroptosis and hyperexcitability in SE mice, AAV-sh-TRPM7 containing with a green fluorescent (EGFP) tag was delivered to C57BL/6 J mice via stereotaxic injection. As shown in Supplemental Fig. 2G, EGFP (green) was expressed in the hippocampus, indicating that the AAV was successfully injected. Protein expression levels of TRPM7 in the hippocampus of AAV-sh-TRPM7-EGFP and AAV-sh-NC-EGFP transfection SE mice was evaluated by western blot (Fig. 3A) and immunofluorescence staining analysis (Supplemental Fig. 3A). TRPM7 levels in the hippocampus of AAV-sh-TRPM7-EGFP transfected mice were reduced compared with AAV-sh-NC-EGFP group (Fig. 3A), where the immunostaining intensity of TRPM7 (Supplemental Fig. 3, A and B) was decreased as well, suggesting that AAV-sh-TRPM7-EGFP transfection reduced PILO-induced TRPM7 expression.

To assess whether AAV-sh-TRPM7-EGFP transfection could affect PILO-induced pyroptosis, the protein expression levels of pyroptosis factors were evaluated by western blot and ELISA. The transfection of AAV-sh-TRPM7-EGFP reduced NLRP3, GSDMD, caspase-1

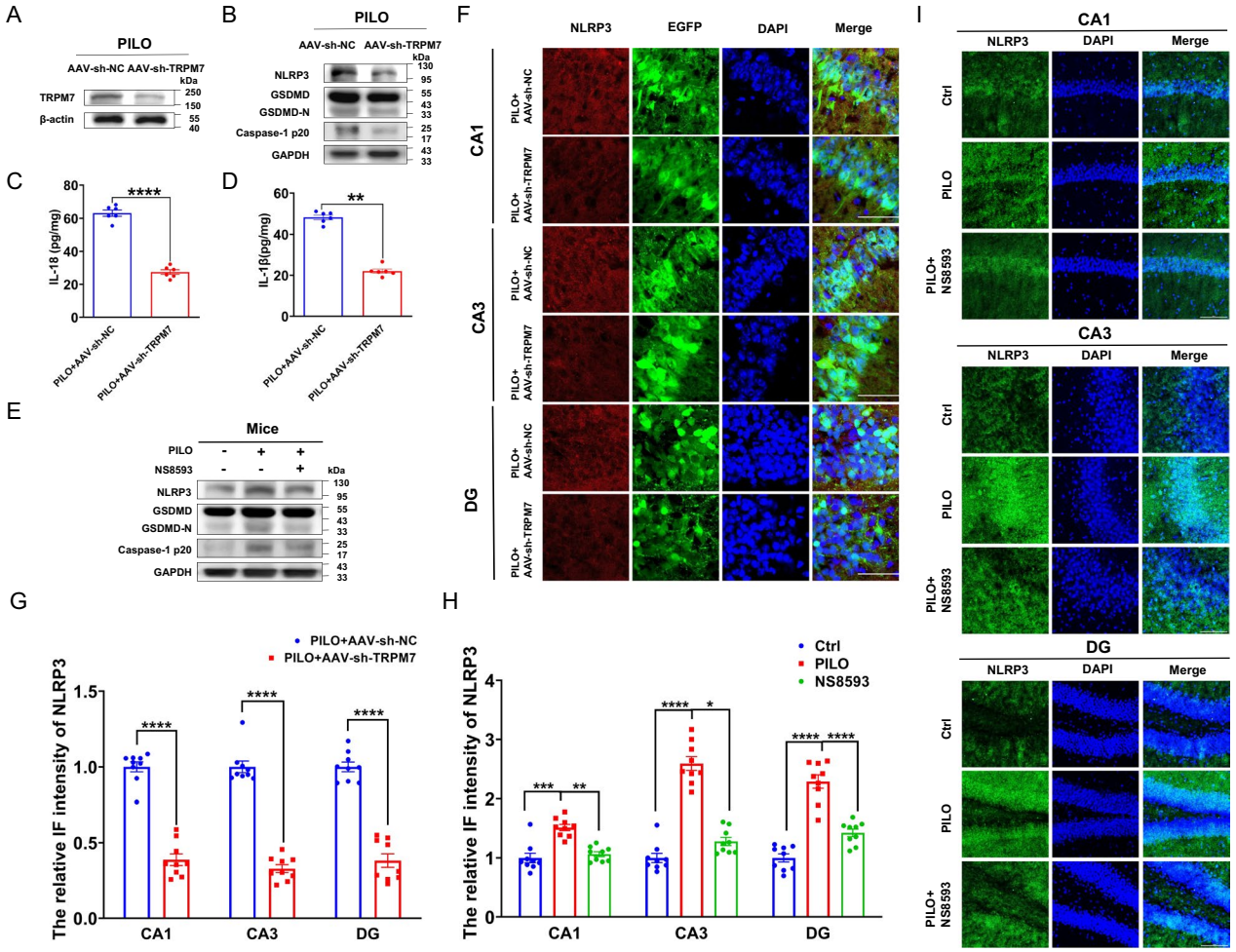

Fig. 3 TRPM7 contributed to pyroptosis in SE models in vivo. **A** The representative protein bands of TRPM7 in the hippocampus of PILO-treated C57BL/6 J mice after AAV-sh-TRPM7-EGFP or AAV-sh-NC-EGFP transfection ($n=6$). **B** The representative protein bands of NLRP3, GSDMD, and caspase-1 p20 of PILO-treated C57BL/6 J mice after AAV-sh-TRPM7-EGFP or AAV-sh-NC-EGFP transfection ($n=5$). **C**, **D** ELISA analysis of IL-18 (C) and IL-1β (D) in hippocampus homogenates of PILO-treated C57BL/6 J mice after AAV-sh-TRPM7-EGFP or AAV-sh-NC-EGFP transfection ($n=6$). **E** The representative protein bands of NLRP3, GSDMD, and caspase-1 p20 expression in hippocampus of PILO-treated C57BL/6 J mice after NS8593 pretreatment ($n=6$). **F**, **G** Immunofluorescence assessment of NLRP3 (red) expression in the hippocampus (120×lens) of PILO-treated C57BL/6 J mice after AAV-sh-TRPM7-EGFP (green) or AAV-sh-NC-EGFP (green) transfection, including the CA1, CA3 and DG regions ($n=9$). Scale bar: 200 μm. DAPI (blue) is used to label nucleus. **H**, **I** Immunofluorescence analysis of NLRP3 (green) expression in hippocampus (40×lens) of PILO-treated C57BL/6 J mice after NS8593 pretreatment, including the CA1, CA3, and DG regions ($n=9$). Scale bar: 500 μm. DAPI (blue) was used to label nucleus. Full scans of all the blots are in the Supplementary Note. *$P<0.05$; **$P<0.01$; ***$P<0.001$; **** $P<0.0001$

p20 (Fig. 3B), IL-18 (Fig. 3C), and IL-1β (Fig. 3D) levels compared with AAV-sh-NC-EGFP transfected mice. The immunostaining intensity of NLRP3 was decreased in the hippocampus including CA1, CA3, and DG regions (Fig. 3, F and G) of AAV-sh-TRPM7-EGFP transfected mice compared with that in the AAV-sh-NC-EGFP transfection group.

To assess the effect of NS8593, a non-specific inhibitor of TRPM7[33], in neuronal damage and pyroptosis in PILO-treated mice, 5 mg/kg NS8593 was applied intravenously 30 min before PILO administration. The PILO group revealed significant up-regulation of NLRP3, GSDMD, and caspase-1 p20 (Fig. 3E) compared with the control group by western blot. Compared with the PILO group, pretreatment with NS8593 group reduced the expression of NLRP3, GSDMD, and caspase-1 p20 ((Fig. 3E). Additionally, NLRP3 was up-regulated in the CA1, CA3, and DG (Fig. 3, H and I) regions. NS8593 pretreatment in PILO-treated group caused a significant reduction of NLRP3 in the CA1, CA3, and DG (Fig. 3, H and I) regions compared with PILO-treated group. These data indicate that silencing TRPM7 and TRPM7

inhibition by NS8593 reduced pyroptosis in PILO-treated SE mice.

TRPM7-mediated Zn^{2+} contributed to pyroptosis

TRPM7 is a high Zn^{2+} permeable ion channel[34]. The abnormal accumulation of intracellular Zn^{2+} can lead to neuron death and brain disorders including epileptic seizures and stroke[35]. In order to evaluate whether the intracellular Zn^{2+} levels were changed in the hippocampus of PILO-treated SE mice, we used the Zn^{2+}-specific stain the N-(6-methoxy-8-quinolyl)-para-toluenesulfonamide (TSQ) to detect the change of intracellular Zn^{2+} accumulation. TSQ fluorescence was observed in the hippocampus CA1, CA3, and DG regions (Fig. 4A). Compared with the control group, higher TSQ fluorescence intensity was detected in the hippocampus CA1, CA3, and DG regions (Fig. 4, A and B) of PILO-treated SE mice. Thus, intracellular Zn^{2+} accumulation was enhanced in the hippocampus of PILO-treated mice.

Next, we checked whether Zn^{2+} can induce pyroptosis in vitro. Here, we treated N2a cells with 30 μM and 100 μM $ZnCl_2$ for 24 h to allow Zn^{2+} influx to the cytoplasm. In western blot experiments, the activation of pyroptosis by Zn^{2+} was dose-dependent (Fig. 4C).

To further investigate the involvement of TRPM7-mediated Zn^{2+} in pyroptosis, we measured the changes of pyroptosis associated factors in empty vector-transfected N2a cells, TRPM7-overexpressed cells after PILO treatment, and TRPM7-overexpressed cells after exposed to PILO combined with TPEN, a membrane-permeable Zn^{2+} chelator. We used 1 μM TPEN to chelate intracellular Zn^{2+} ($K_{d\ Zn}=0.7$ fM) following the same treatment regimen as previously shown[36]. After PILO treatment, the protein levels of NLRP3, GSDMD, and caspase-1 p20 (Fig. 4D) were significantly enhanced in TRPM7-overexpressed cells. In TRPM7-overexpressed N2a cells, PILO combined with TPEN treatment remarkably down-regulated the protein levels of NLRP3, GSDMD, and caspase-1 p20 (Fig. 4D). Thus, the application of TPEN reversed pyroptosis via TRPM7.

TPEN also has high affinity to Fe^{2+}($K_{d\ Fe}=2.4$ fM) and Cu^{2+} ($K_{d\ Cu}=17$ zM)[37]. To verify whether TRPM7-mediated Fe^{2+} or Cu^{2+} participates in pyroptosis, we applied the iron chelator deferoxamine (DFX)[38] and the specific Cu^{2+} chelator tetrathiomolybdate (TTM)[39]. In TRPM7-overexpressed cells, treatment with 1 μM TPEN down-regulated the protein levels of NLRP3, GSDMD, and caspase-1 p20 (Fig. 4E). Nevertheless, exposure to 2 μM DFX and 1 μM TTM failed to diminish the expression of these pyroptosis associated factors in TRPM7-overexpressed cells (Fig. 4E), suggesting that Zn^{2+} rather than Fe^{2+} or Cu^{2+} was involved in TRPM7-mediated pyroptosis.

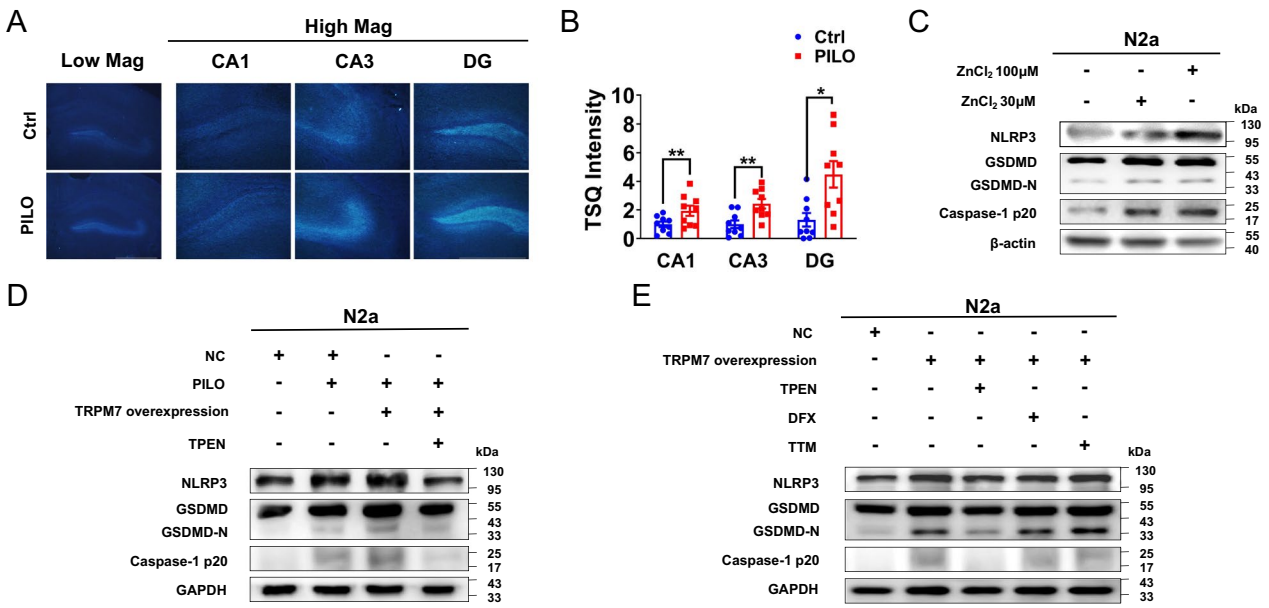

Fig. 4 TRPM7-mediated Zn^{2+} contributed to pyroptosis. **A** The TSQ staining detected in hippocampus (4 × lens) of PILO-treated C57BL/6 J mice, including the enlarged CA1, CA3 and DG regions (10 × lens). Scale bar: 500 μm. **B** Statistical analysis of TSQ intensity ($n=9$). **C** The representative protein bands of NLRP3, GSDMD, and caspase-1 p20 in N2a cells treated with $ZnCl_2$ (30 μM and 100 μM) ($n=6$). **D** The representative protein bands of NLRP3, GSDMD, and caspase-1 p20 in PILO-treated N2a cells after TRPM7 overexpression and TPEN (1 μM) pretreatment ($n=5$ or 6). **E** The representative protein bands of NLRP3, GSDMD, and caspase-1 p20 in TRPM7-overexpressed N2a cells after TPEN(1 μM), DFX(1 μM), or TTM(1 μM) pretreatment ($n=6$). Full scans of all the blots are in the Supplementary Note. *$P < 0.05$; **$P < 0.01$

P-STAT3 promoted both Trpm7 and Nlrp3 transcription in PILO-treated N2a cells

STAT3 is a member of the signal transducer and activator of transcription (STAT) family, and it is activated by tyrosine phosphorylation, translocating from the cytoplasm to the nucleus to mediate the transcription of target genes[40]. The protein levels of STAT3, p-STAT3 and p-STAT3/STAT3 were increased in PILO-treated animals[41–43]. Here, we used RNA sequencing to explore the DEGs associated with PILO treatment. KEGG analysis disclosed that the up-regulated genes were mainly enriched in members of the JAK-STAT signaling pathway, which is the TOP 5 items of KEGG (Fig. 5A). In PILO-treated N2a cells, we found that STAT3 phosphorylation inhibitor Stattic reversed PILO-treated up-regulation of NLRP3 (Fig. 5, B and C), indicating that NLRP3 was up-regulated in PILO-treated SE model via p-STAT3 signaling.

We then hypothesized that p-STAT3 could promote the transcription of *Nlrp3* and *Trpm7*. ChIP assay was applied to verify the interaction of p-STAT3 protein with the *Nlrp3* and *Trpm7* genes. We performed JASPAR database analysis to predict binding sites between STAT3 and promoters of *Trpm7* and *Nlrp3*, and designed three pairs of primers for ChIP-qPCR assay (Fig. 5D and Supplemental Fig. 4A). Here, p-STAT3 was specifically recruited to the GTGCGGGAAG region of *Trpm7* after PILO treatment (Fig. 5D). Additionally, STAT3 recruitment to the TTACAGTAAA region of *Trpm7* was augmented in the the PILO-treated group specifically (Supplemental Fig. 4A). Similarly, the recruitment of p-STAT3 to the TTCTGGGATG region of *Nlrp3* was enhanced in PILO treated N2a cells (Fig. 5D) compared with the normal N2a cells. There was no recruitment of p-STAT3 to the other two regions (Fig. 5D). STAT3 was also recruited to the *Nlrp3* promoter region of CTTCCTGTCT in the absence (Supplemental Fig. 4A) of PILO. Collectively, our results suggest that STAT3 or p-STAT3 was recruited to the promoter region of *Trpm7* and *Nlrp3*, thereby activating *Trpm7* and *Nlrp3* transcription in PILO-treated cells.

TRPM7 contributed to pyroptosis via *the Zn^{2+}/ROS/JAK2/STAT3 pathway in SE*

To explore the function of STAT3 in SE, we evaluated STAT3 activation by measuring the relative level of STAT3 Tyr705 phosphorylation (pY^{705}-STAT3) using western blot analysis. Here, levels of pY^{705}-STAT3/STAT3 were enhanced in the total, cytosolic, and nuclear fractions (Fig. 6, A and B) of PILO-treated N2a cells, suggesting that p-STAT3 upregulation was apparent in the nucleus and cytoplasm.

To understand the relationship between TRPM7-mediated Zn^{2+} and STAT3, we detected the relative levels of pY^{705}-STAT3/STAT3 in empty vector-transfected N2a cells, TRPM7-overexpressed cells after PILO treatment, and TRPM7-overexpressed cells after exposure to PILO and 1 μM TPEN. The results indicated that after PILO treatment, the protein expression of pY^{705}-STAT3/STAT3 (Fig. 6, C and D) were significantly enhanced in TRPM7-overexpressed cells, while TPEN treatment diminished the expression of pY^{705}-STAT3/STAT3 (Fig. 6, C and D). In TRPM7-overexpressed N2a cells, exposure to 2 μM DFX and 1 μM TTM did not attenuate the elevated protein levels of pY^{705}-STAT3/STAT3 (Fig. 6, E and F). Meanwhile, the influx of Zn^{2+} into the cytoplasm also enhanced the protein expressions of pY^{705}-STAT3/STAT3 (Fig. 6, G and H). Thus, TRPM7-mediated Zn^{2+} contributed to STAT3 activation in PILO-treated N2a cells.

Disturbances in cellular Zn^{2+} levels are toxic to N2a cells and Zn^{2+} is related to the generation of reactive oxygen species (ROS)[44]. To assess oxidative stress of TRPM7-Zn^{2+}-induced pyroptosis, mitochondrial membrane potential (MMP) and ROS production were examined in N2a cells treated with PILO, PILO combined with TRPM7 siRNA transfection, or PILO combined with 1 μM TPEN with the JC-1 and DCFH-DA dyes (fluorescent probe 2,7-Dichlorodi-hydrofluorescein diacetate (DCFH-DA)). Here, the intracellular ROS was up-regulated in N2a cells treated with PILO for 24 h (Fig. 6, I and K). Additionally, the si-TRPM7 and TPEN treatment significantly reduced the up-regulation of ROS (Fig. 6, I and K). Similarly, the treatment of si-TRPM7 or TPEN inhibited the decreased mitochondrial potential in N2A cells treated with PILO compared with the control group (Fig. 6, J and L), indicating that knockdown of TRPM7 or TPEN treatment inhibited oxidative stress responses in PILO-treated N2a cells.

Moreover, when N2a cells were pre-treated with the ROS scavenger NAC[45] and JAK2 inhibitor AG490[46] and then treated with PILO, pyroptosis associated protein expression, as well as the activation of JAK2/STAT3 were suppressed (Fig. 6M). In addition, the STAT3 phosphorylation inhibitor Stattic reversed PILO-treated up-regulation of the relative levels of pyroptosis indicators (Fig. 6M) but did not affect the protein level of p-JAK2/JAK2 (Fig. 6, M and N). Additionally, the protein levels of pY^{705}-STAT3/STAT3 in PILO-treated cells were significantly higher than control group. This effect was inhibited by NAC, AG490, and Stattic treatment (Fig. 6, M and N). Thus, TRPM7 contributed to pyroptosis via the Zn^{2+}/ROS/JAK2/STAT3 pathway in SE.

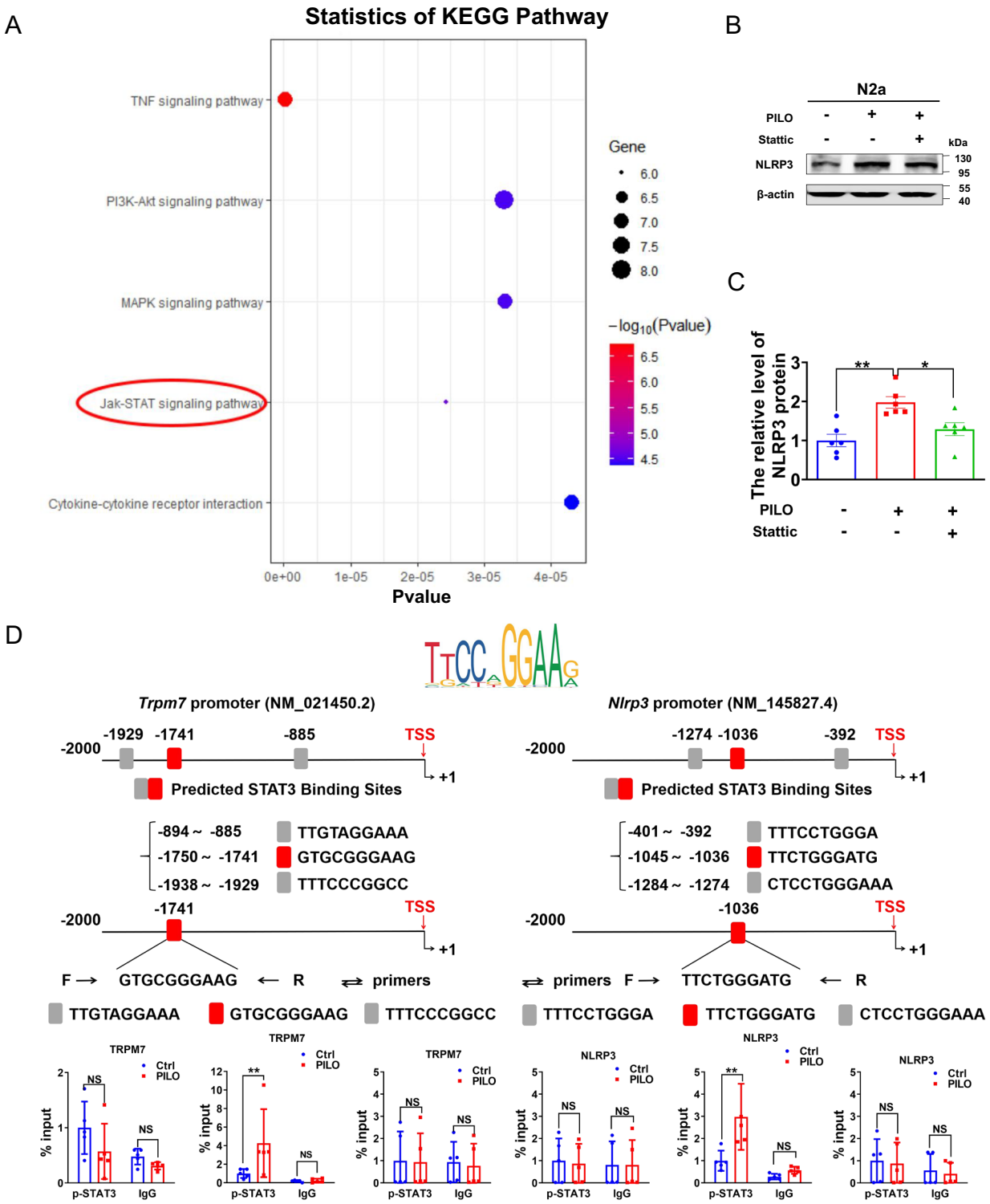

Fig. 5 P-STAT3 promoted the transcription of *Trpm7* and *Nlrp3* in PILO-treated N2a cells. KEGG pathway analysis revealed that the up-regulated genes in DEGs between control C57BL/6mice and PILO-treated mice were involved in many signaling pathways, including JAK-STAT signaling pathway, which is the TOP 5 items of KEGG ($n = 5$). **B**, **C** The representative protein bands (B) and data analysis of NLRP3 (C) in N2a cells treated with PILO alone or combined with Stattic (0.5 μM) pretreatment ($n = 6$). **D** Top: P-STAT3 was recruited to the promoter regions of *Trpm7* and *Nlrp3*. The sequence logo of potential STAT3 binding sites in the *Trpm7* or *Nlrp3* sequence in JASPAR. Bottom: ChIP assays performed on the promoter regions of *Trpm7* or *Nlrp3* with the p-STAT3 antibodies in N2a cells with or without PILO (10 μM) treatment ($n = 5$). TSS indicates transcription start site. Full scans of all the blots are in the Supplementary Note. * $P < 0.05$; ** $P < 0.01$; NS not significant

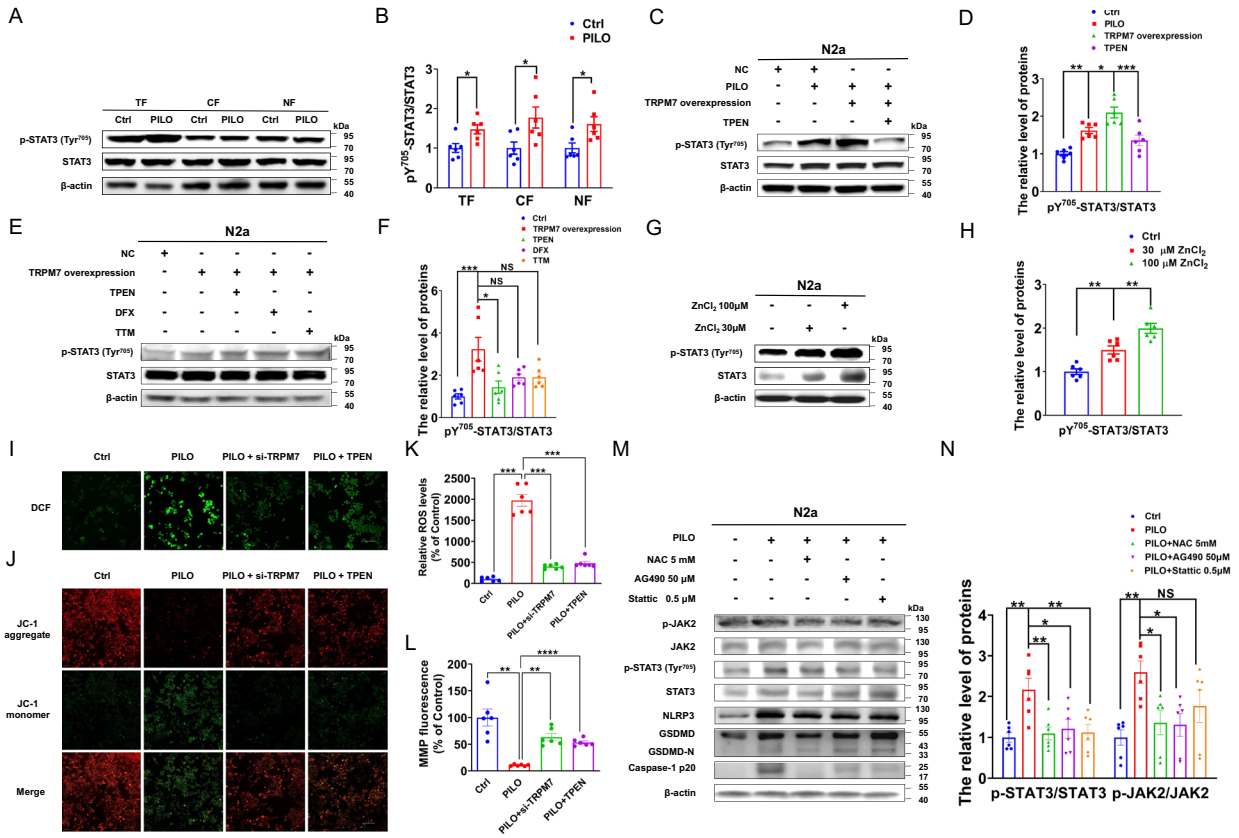

Fig. 6 TRPM7 participated in pyroptosis via the Zn^{2+}/ROS/JAK2/STAT3 pathway in SE. **A**, **B** The representative protein bands (A) and data analysis of STAT3 and pY^{705}-STAT3/STAT3 (B) in the total fractions (TF), cytosolic fractions (CF), and nuclear fractions (NF) of PILO-treated N2a cells ($n=6$). **C**, **D** The representative protein bands (C) and data analysis of STAT3 and pY^{705}-STAT3/STAT3 (D) in PILO-treated N2a cells after TRPM7 overexpression and TPEN (1 μM) pretreatment ($n=6$). **E**, **F** The representative protein bands (E) and data analysis of STAT3 and pY^{705}-STAT3/STAT3 (F) in TRPM7-overexpressed N2a cells after TPEN(1 μM), DFX(1 μM), or TTM(1 μM) pretreatment ($n=6$). **G**, **H** The representative protein bands (G) and data analysis of STAT3 and pY^{705}-STAT3/STAT3 (H) in N2a cells treated with $ZnCl_2$ (30 μM and 100 μM) ($n=6$). **I-L** ROS and MMP production were measured by DCFH-DA dying or JC-1 in PILO-treated N2a cells after TRPM7 knockdown or TPEN (1 μM) pretreatment ($n=6$). Scale bar: 100 μm. **M**, **N** The representative protein bands (M) and data analysis of NLRP3, GSDMD, caspase-1 p20, pY^{705}-STAT3/STAT3, p-JAK2/JAK2, STAT3, and JAK2 (N) in PILO-treated N2a cells after NAC (5 mM), AG490 (50 μM) or Stattic (0.5 μM) pretreatment ($n=6$). Full scans of all the blots are in the Supplementary Note. * $P<0.05$; ** $P<0.01$; *** $P<0.001$; **** $P<0.0001$; NS not significant

Sliencing TRPM7 and TRPM7 inhibition by NS8593 alleviated neuronal damage in PILO-treated SE mice

We determined the effect of AAV-sh-TRPM7-EGFP transfection on PILO-induced neuronal damage. Astrocytes respond to neuronal damage by proliferating and modulating their activity[47]. Here, we investigated the distribution of neurons labeled by NeuN and that of astrocytes labeled by glial fibrillary acidic protein (GFAP) in the hippocampus. AAV-sh-TRPM7-EGFP transfection markedly reduced the immunostaining intensity of GFAP (Supplemental Fig. 3, C and D) and increased the number of neurons (Fig. 7 A, B) compared with those of the AAV-sh-NC-EGFP transfected mice, indicating the critical role of TRPM7 in mediating PILO-induced neuronal damage.

Meanwhile, we assessed the effect of NS8593 in neuronal damage in PILO-treated mice (Fig. 7F). Compared with the control group, the number of neurons was reduced in CA1, CA3, and DG regions (Fig. 7, D, F) of hippocampus in PILO-treated SE mice. When compared with PILO-treated mice, NS8593 pretreatment with PILO (PILO + NS8593) showed the increasing number of neurons in CA1, CA3, and DG regions (Fig. 7 D, F). In addition, compared with the control group, GFAP intensity changes were confirmed in CA1, CA3, and DG regions (Fig. 7 E, F) in the hippocampus of PILO-treated mice. NS8593 pretreatment remarkably reduced the intensity of GFAP in CA1, CA3, and DG regions (Fig. 7 E, F) of hippocampus compared with those of the PILO-treated group.

Additionally, NeuN protein levels were decreased (Fig. 7C) and GFAP protein levels were significantly

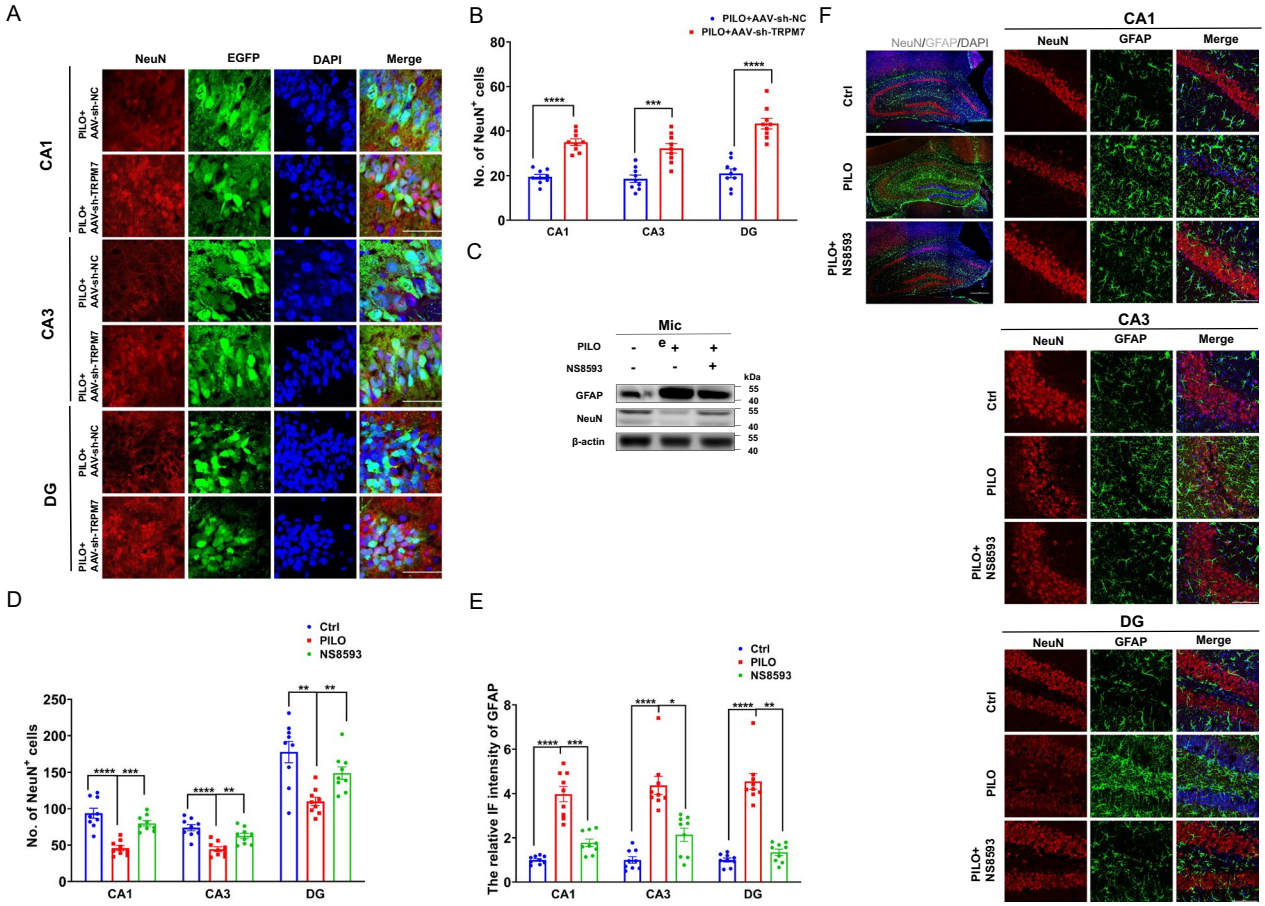

Fig. 7 Silencing TRPM7 and TRPM7 inhibition by NS8593 mitigated neuronal damage and pyroptosis in SE mice. **A**, **B** Immunofluorescence analysis of NeuN (red) expression in the hippocampus (120 × lens) of PILO-treated C57BL/6 J mice after AAV-sh-TRPM7-EGFP (green) or AAV-sh-NC-EGFP (green) transfection, including the CA1, CA3 and DG regions ($n = 9$). Scale bar: 200 μm. DAPI (blue) is used to label nucleus. **C** The representative protein bands of NeuN and GFAP in hippocampus of PILO-treated C57BL/6 J mice after NS8593 pretreatment ($n = 6$). **D-F** Immunofluorescence analysis of NeuN (red) and GFAP (green) expression in hippocampus (10 × lens) of PILO-treated C57BL/6 J mice after NS8593 pretreatment, including the enlarged CA1, CA3, and DG regions (40 × lens) ($n = 9$). Scale bar: 100 μm and 500 μm. DAPI (blue) was used to label nucleus. Full scans of all the blots are in the Supplementary Note. *$P < 0.05$; ** $P < 0.01$; *** $P < 0.001$; **** $P < 0.0001$

increased (Fig. 7C) in PILO-treated SE mice. The PILO + NS8593 group showed decreased GFAP protein levels (Fig. 7C) and increased levels of NeuN (Fig. 7C). Thus, silencing TRPM7 and TRPM7 inhibition by NS8593 suppressed neuronal damage and neuronal death in PILO-treated SE mice.

Silencing TRPM7 and TRPM7 inhibition by NS8593 reversed neuronal hyperexcitability in PILO-treated SE models

We evaluated the impact of AAV-sh-TRPM7-EGFP transfection in an in vivo SE model by EEG. Flowcharts of the injection protocol is shown in Supplemental Fig. 5A. Representative EEG recordings are shown in Fig. 8A. Based on EEG recordings, we found the mean total duration of seizure activity was decreased in the group pretreated with AAV-sh-TRPM7-EGFP (median score on the Racine scale was 2) compared with the group using vector and PILO (median score on the Racine scale was 4.5) (Fig. 8, A and B), implying that TRPM7 has a crucial role in regulating PILO-induced hyperexcitability. Therefore, TRPM7 knockdown lessened neuronal damage and pyroptosis and reversed disease associated neuronal hyperexcitability.

We investigated the effect of TRPM7 inhibitor NS8593 and NLRP3 inflammasome inhibitor MCC950 in PILO-induced neuronal excitability of in vitro models and in vivo models of SE by patch clamp and EEG. We first applied 10 μM of PILO for the in vitro neuronal models by patch clamp as in previous studies[48]. We found that the number of spontaneous action potentials (APs) (Fig. 8 C, D) and evoked APs firing measurements (Fig. 8 C ,E) in the PILO-treated hippocampal neurons were more frequent than those of the control group. However, compared with the PILO-treated hippocampal

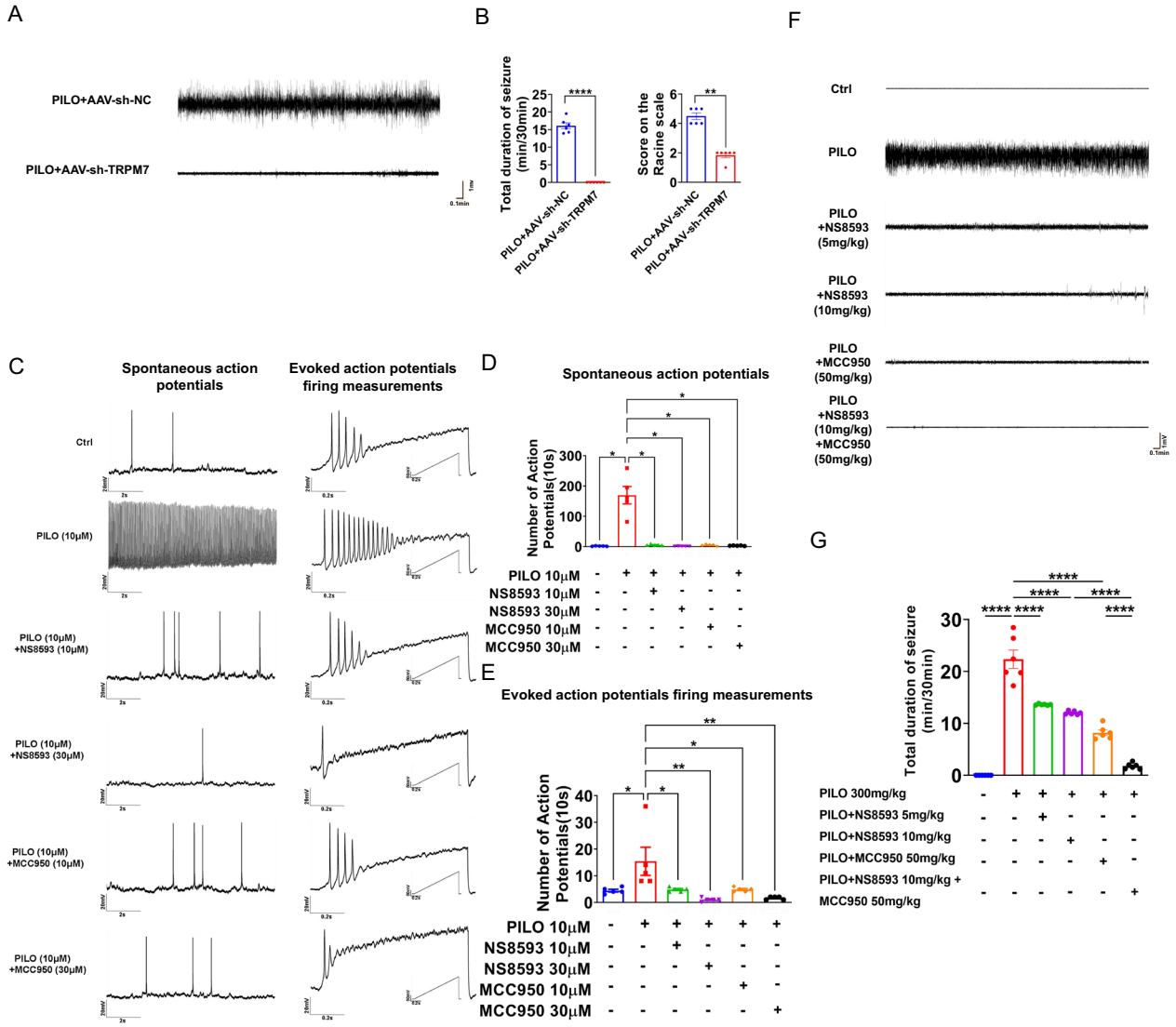

Fig. 8 Silencing TRPM7 and TRPM7 inhibition reversed the hyperexcitability in the SE models. **A** Representative 5 min EEG recording showing seizure onset. The mice were stereotaxically injected with AAV-sh-TRPM7-EGFP or AAV-sh-NC-EGFP, followed by PILO induction 1 month later. EEG was conducted right after the induction of PILO, and the recording time was 0.5 h. **B** Left: The mean total duration of seizure activity in PILO-treated C57BL/6 J mice after AAV-sh-TRPM7-EGFP or AAV-sh-NC-EGFP transfection ($n = 6$). Right: The score on the Racine scale. **C** The representative traces of occasional spontaneous APs (left) and APs evoked by injecting a 1-s depolarizing currents with a maximum of 200 pA in a ramp mode. and the number of two types of APs were compared between the PILO (10 μM) group and the control group, as well as the NS8593 (10 μM and 30 μM) + PILO group and the PILO group, and the MCC950 (10 μM and 30 μM) + PILO group and the PILO group. **D**, **E** Statistical analysis of the number of spontaneous APs and APs evoked by injecting depolarizing currents. **F** Representative 5 min EEG recording showing seizure onset. The mice were injected with NS8593 or MCC950 or both, followed by PILO 0.5 h later. **G** The mean total duration of seizure activity in control, PILO-treated, NS8593-pretreated (5 mg/kg), NS8593-pretreated (10 mg/kg), MCC950-pretreated (50 mg/kg) and NS8593 (10 mg/kg) combined with MCC950-pretreated (50 mg/kg) mice ($n = 6$). * $P < 0.05$; ** $P < 0.01$; **** $P < 0.0001$

neurons, the NS8593 (10 μM and 30 μM) pretreatment combined with PILO treatment group (PILO + NS8593) significantly attenuated spontaneous APs (Fig. 8 C, D) and evoked APs (Fig. 8 C, E). Similarly, the number of spontaneous APs (Fig. 8 C, D) and evoked APs (Fig. 8 C, E) in the MCC950 (10 μM and 30 μM) pretreatment combined with PILO treatment group (PILO + MCC950) were increased compared with those in the PILO-treated cultured hippocampal neurons.

Next, we determined whether NS8593 and MCC950 altered neuronal excitability in the in vivo model of SE. Flowchart of the injection protocol is shown in Supplemental Fig. 5B. Representative EEG recordings are shown in Fig. 8F. We found that the mean total duration

of seizure activity in the mice pretreated with NS8593 (5 mg/kg and 10 mg/kg i.v.) was significantly decreased compared to the group with PILO alone (Fig. 8, F and G). Similarly, the duration of seizure activity in the group pretreated with MCC950 (50 mg/kg i.p.) was significantly decreased compared to the group with PILO treatment (Fig. 8 F, G). The duration of seizure activity in co-administration of NS8593 and MCC950 was decreased significantly compared to PILO + NS8593 group (Fig. 8 F, G) and PILO + MCC950 group, respectively. Thus, NS8593 and MCC950 ameliorated the increased neuronal excitability induced by PILO, indicating that the pharmacological inhibitors of TRPM7 and NLRP3 reversed hyperexcitability in vivo.

TRPM7 conditional knockout mice alleviated neuronal damage and pyroptosis and reversed PILO-treated neuronal hyperexcitability

We successfully generated TRPM7 conditional knockout (CKO) mice by crossing $TRPM7^{f/f}$ mice with Cre transgenic mice (Supplemental Fig. 5C). In TRPM7-CKO mice, TRPM7 expression was significantly reduced in the hippocampus, compared to floxed controls, as confirmed by western blot (Fig. 9, A and B). Indeed, as shown in Supplemental Fig. 5D, PILO-treated TRPM7-CKO mice exhibited lower amount of $TRPM7^{+}$ cells in $NeuN^{+}$ neurons in CA1, CA3, and DG regions.

In addition, we found the mean total duration of seizure activity was decreased in TRPM7-CKO mice (median score on the Racine scale was 1.5) compared with $TRPM7^{f/f}$ mice (median score on the Racine scale was 4.5) (Fig. 9 E, F). Moreover, compared with $TRPM7^{f/f}$ mice, the protein levels of NLRP3, GSDMD, and caspase-1 p20 (Fig. 9 C,D) were significantly decreased in TRPM7-CKO mice. The immunostaining intensity of NLRP3 were lower in CA1, CA3, and DG (Fig. 9 G, H) regions in hippocampus of TRPM7-CKO mice than that of $TRPM7^{f/f}$ mice. Meanwhile, the loss of neurons and the increased intensity of GFAP after SE were significantly alleviated in TRPM7-CKO mice (Fig. 9 I–K). Therefore, the TRPM7 conditional knockout mice alleviated neuronal damage and pyroptosis and reversed PILO-treated neuronal hyperexcitability.

The TRPM7 inhibitor, SDUY-225, reducesd pyroptosis, neuronal damage, and hyperexcitability in SE mice

SDUY-225 was a new compound designed according to the structure of NS8593 (Fig. 10A). We assessed the efficacy of SDUY-225 to inhibit TRPM7 channel activity in whole-cell patch-clamp experiments conducted with HEK293 cells overexpressing TRPM7[49]. Measuring the outward current amplitude at + 80 mV shows that the current amplitude increases to near full activation over ~ 140 s (Fig. 10B), after which various concentrations of SDUY-225 were applied extracellularly. These currents are characterized by steep outward rectification due to small divalent cation permeation at negative membrane voltages and gradually increasing outward conductance of monovalent cations (Cs^{+} ions, Fig. 10C). This caused a concentration-dependent inhibition of TRPM7 outward currents and the analysis of this behavior at 340 s into the experiment yielded a concentration–response curve with IC_{50} of 1.7 μM and cooperativity Hill coefficient of 2.8 (Fig. 10D).

To verify the pharmacological effect of SDUY-225, we applied low-dose and high-dose SDUY-225 to PILO-treated C57BL/6 J (2.5 mg/kg i.v. and 5 mg/kg i.v.) and N2a cells (1.7 μM and 2.5 μM). Compared with the PILO treated group, pretreatment with low-dose SDUY-225, the expression of NLRP3, GSDMD, caspase-1 p20 (Fig. 10E), IL-18 (Fig. 10F), and IL-1β (Fig. 10G) were reduced, as the immunostaining intensity of NLRP3 were decreased in the CA1, CA3, and DG (Supplemental Fig. 6A) regions compared with that in the hippocampus of PILO-treated mice. High-dose SDUY-225 pretreatment in the PILO-treated group caused a significant reduction of NLRP3, GSDMD, caspase-1 p20 (Fig. 10E), IL-18 (Fig. 10F), and IL-1β (Fig. 10G) expression. In addition, the immunostaining intensity of NLRP3 was also decreased in the CA1, CA3, and DG (Supplemental Fig. 6A) regions compared with that in the hippocampus of PILO-treated mice. The pyroptosis associated indicators in the hippocampus of PILO-treated mice treated with high-dosage of SDUY-225 were decreased compared with those in hippocampus of PILO-treated mice pretreated with NS8593. Additionally, high-dose SDUY-225 pretreatment in PILO-treated N2a cells also caused a significant reduction in the expression of NLRP3, GSDMD, caspase-1 p20 (Fig. 10H), IL-18 (Fig. 10I), and IL-1β (Fig. 10J), suggesting that TRPM7 new inhibitor SDUY-225 could alleviate pyroptosis in PILO-treated SE models.

Compared with the PILO-treated group, the number of neurons was increased in CA1, CA3, and DG (Supplemental Fig. 7A) hippocampal regions in PILO-treated mice after pretreatment with low-dose SDUY-225. Compared with the untreated group, high-dose SDUY-225 pretreatment showed an increased number of neurons in CA1, CA3, and DG (Supplemental Fig. 7A) regions. In addition, the decreased GFAP expression was observed in CA1, CA3, and DG (Supplemental Fig. 7A) regions in hippocampus of low-dosage of SDUY-225 pretreated SE mice. Moreover, the high-dose SDUY-225 pretreatment reduced GFAP expression in CA1, CA3, and DG (Supplemental Fig. 7A) regions of the hippocampus compared with those of untreated group.

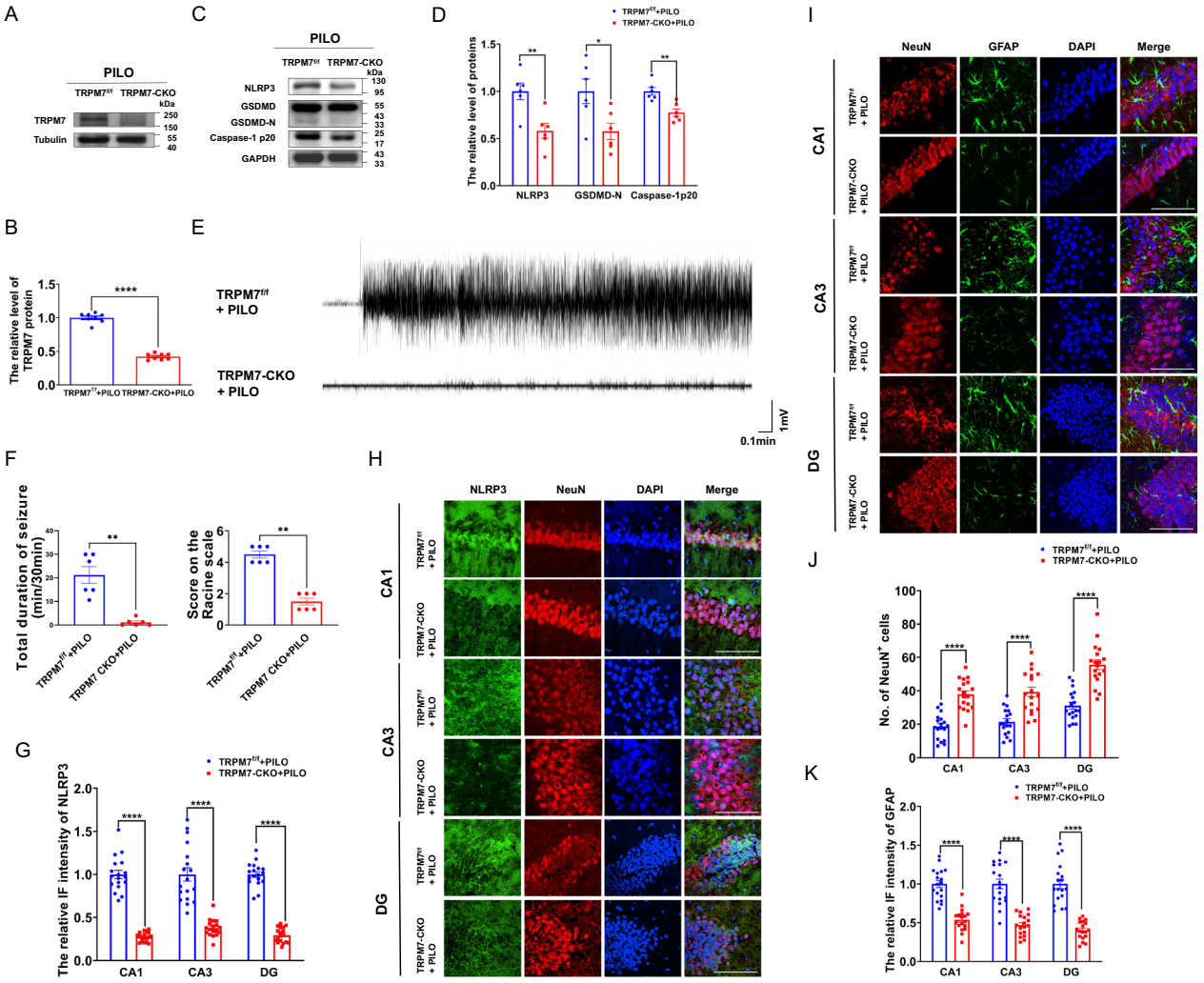

Fig. 9 TRPM7 conditional knockout mice reduced neuronal damage and pyroptosis and reversed PILO-treated neuronal hyperexcitability. **A**, **B** The representative protein bands and analysis of TRPM7 in hippocampus of TRPM7-CKO mice ($n=6$). **C**, **D** The representative protein bands and analysis of NLRP3, GSDMD, and caspase-1 p20 in hippocampus of TRPM7-CKO mice ($n=6$). **E** Representative 5 min EEG recording showing seizure onset. The TRPM7-CKO mice were injected with PILO. **F** Left: The mean total duration of seizure activity in PILO-treated TRPM7-CKO mice ($n=6$). Right: The score on the Racine scale. **G**, **H** Immunofluorescence analysis of NLRP3 (green) and NeuN (red) expression in hippocampus of PILO-treated C57BL/6 J mice (100 × lens), including the CA1, CA3 and DG regions ($n=18$). Scale bar: 100 μm. DAPI (blue) was used to label nucleus. **I-K** Immunofluorescence analysis of NeuN (red) and GFAP (green) expression in hippocampus (100 × lens) of PILO-treated TRPM7-CKO mice, including the CA1, CA3, and DG regions ($n=18$). Scale bar: 100 μm. DAPI (blue) was used to label nucleus. Full scans of all the blots are in the Supplementary Note. * $P<0.05$; ** $P<0.01$; **** $P<0.0001$

Finally, we used EEG to determine the pharmacological effect of SDUY-225 in an in vivo SE model. The duration of seizure activity was diminished in a dose-dependent manner in both the low- and high-dosage of SDUY-225 (2.5 mg/kg i.v. and 5 mg/kg i.v.) groups particularly in comparison to the PILO alone group (Fig. 10K). The mean total period of epileptic seizures was decreased in the SDUY-225-pretreatment group (5 mg/kg i.v.) compared to the NS8593 (5 mg/kg i.v.) group (Fig. 10K). Hence, this new TRPM7 inhibitor lessened PILO-treated SE and was more effective than NS8593.

Discussion

Our study provides a novel molecular mechanism of pyroptosis in SE, highlighting the importance of TRPM7 specifically. Our main findings are as follows: (1) TRPM7 contributes to pyroptosis. (2) STAT3-TRPM7-Zn^{2+}-STAT3, as a signaling loop, triggered pyroptosis in SE. (3)

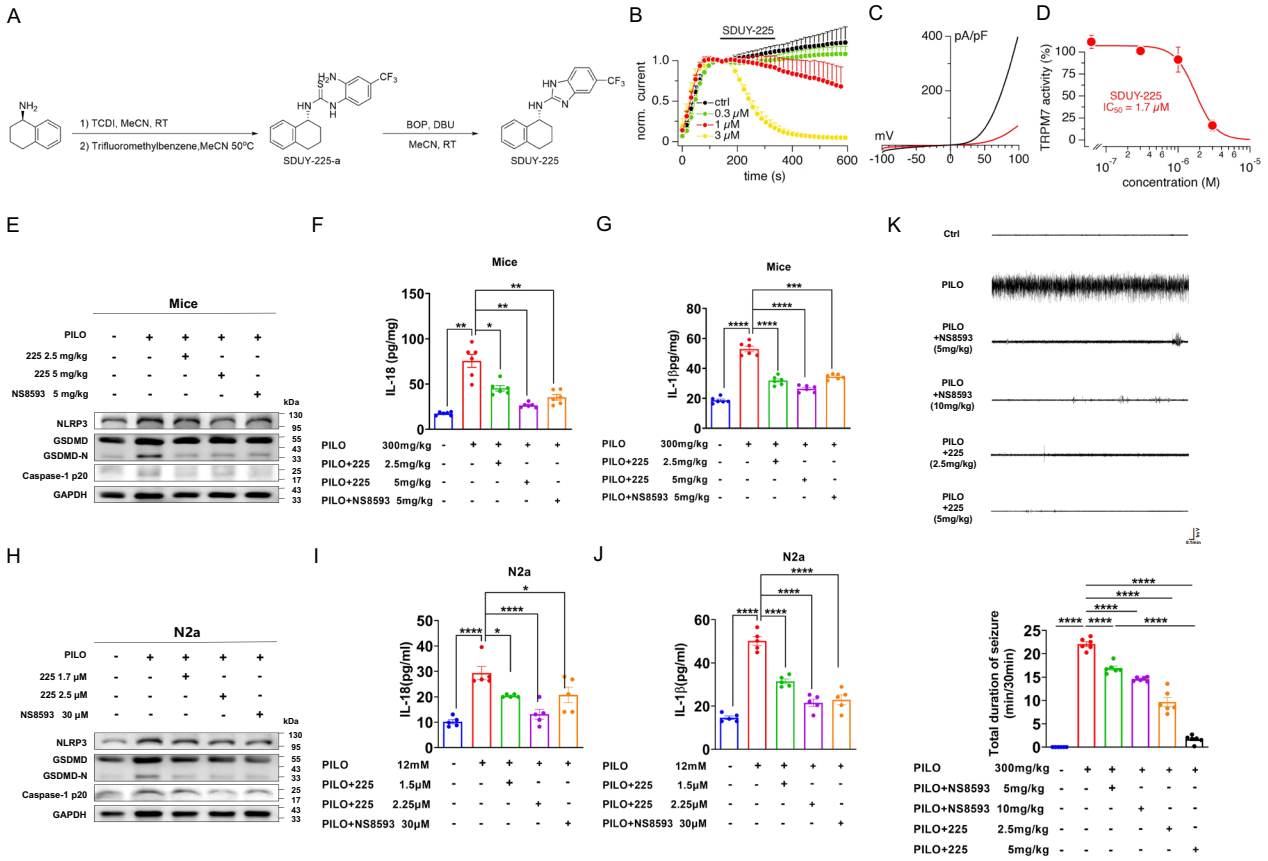

Fig. 10 The TRPM7 inhibitor, SDUY-225, alleviated pyroptosis, neuronal damage, and hyperexcitability in SE mice. **A** Synthesis of SDUY-225. **B-D** Inhibitory effects of 225 on TRPM7 currents were investigated using whole-cell patch-clamp recordings. **B** Average TRPM7-mediated outward currents at + 80 mV extracted from ramp currents delivered at 0.5 Hz and plotted as a function of time ($n = 5$). For clarity, data points are plotted at intervals of 16 s (every 8th ramp). Various concentrations of 225 were applied at 140 s (black bar). Control solution (0 225) contained DMSO vehicle. **C** Current–voltage (I/V) curves extracted from TRPM7 currents evoked in a representative cell by voltage ramps before (138 s, black) and after (340 s, red) 225 application (3 μM). **D** Concentration–response curve obtained by plotting the average TRPM7 amplitudes obtained from data shown in (B). **E** The representative protein bands of NLRP3, GSDMD, and caspase-1 p20 expression in hippocampus of PILO-treated C57BL/6 J mice after 225 (low-dosage and high-dosage) or NS8593 pretreatment ($n = 6$). **F, G** ELISA analysis of IL-18 (F) and IL-1β (G) in hippocampus homogenates of PILO-treated C57BL/6 J mice after 225 (low-dosage and high-dosage) or NS8593 pretreatment ($n = 6$). **H** The representative protein band of NLRP3, GSDMD, and caspase-1 p20 expression in PILO-treated N2a cells after 225 (low-dosage and high-dosage) or NS8593 pretreatment ($n = 6$). **I, J** ELISA analysis of IL-18 (I) and IL-1β (J) in supernatants of PILO-treated N2a cells after 225 (low-dosage and high-dosage) or NS8593 pretreatment. ($n = 5$). **K** Representative 5 min EEG recording showing seizure onset. The mean total duration of seizure activity in PILO-treated C57BL/6 J mice after 225 (low-dosage and high-dosage) or NS8593 pretreatment ($n = 6$). Full scans of all the blots are in the Supplementary Note. *$P < 0.05$; **$P < 0.01$; ***$P < 0.001$; **** $P < 0.0001$

The new inhibitor of TRPM7, SDUY-225, reversed neuronal damage and hyperexcitability in SE.

The pyroptosis-related proteins NLRP3, caspase-1, and IL-1β have been observed to be up-regulated in the pentylenetetrazole (PTZ) kindling model, amygdala kindling model, PILO model, as well as in the hippocampus of temporal lobe epilepsy patients [10, 11, 50, 51]. The protein levels of IL-18 and GSDMD-N were also increased in the PTZ kindling model [12]. Here we show that the expression of pyroptosis-related indicators was increased in models of SE. Meanwhile, GFAP expression was increased and NeuN expression were reduced in PILO-treated SE mice, suggesting that neuronal damage and death occurred in this model. Therefore, our in vivo and in vitro data strongly show that pyroptosis is a crucial cell death modality in SE.

TRPM7 is a nonselective cation channel and abundantly expressed in brain, kidney, spleen, and heart [52]. TRPM7 is permeable to extracellular divalent cations including Zn^{2+}, Ca^{2+} and Mg^{2+}. TRPM7 participates in a range of physiological processes including synaptogenesis and neurite outgrowth, regulation of synapse density,

synaptic plasticity, the maintenance of cognitive functions, and the differentiation and survival of neurons [53]. Moreover, an association of TRPM7 with Alzheimer's disease, Parkinson's disease, and amyotrophic lateral sclerosis (ALS) [19]. Jeong's group firstly found the up-regulation of TRPM7 protein in PILO-treated epileptic rats [54]. TRPM7 inhibitors, carvacrol and 2-APB, suppressed TRPM7 expression and reduced glial activation and neuronal death [21]. Here, TRPM7 was up-regulated in PILO-treated N2a cells, Mg^{2+}-free treated hippocampal neurons, and the hippocampus of PILO-treated SE animal models, indicating that TRPM7 is vital target during epileptogenesis.

One of our impressive findings is that TRPM7 contributes to pyroptosis. By manipulating the expression level of TRPM7 with si-RNA and an overexpression plasmid, we show that TRPM7 acts as an upstream signal to induce pyroptosis. In addition, pretreating with the TRPM7 inhibitor NS8593, and transfection with AAV-sh-TRPM7 reversed the up-regulation of pyroptosis-related proteins in PILO-treated SE mice, suggesting that TRPM7 participates in pyroptosis in SE both in vivo and in vitro. Similarly, the NLRP3 inflammasome inhibitor MCC950 was been observed to reduce the up-regulation of cleaved-caspase-1, IL-1β, and IL-18 in hippocampus of KA-treated SE mice [55]. Thus, NS8593 and NLRP3 inflammasome inhibitor MCC950 can reduce the hyperexcitability both in PILO-treated hippocampal neurons and SE mice, revealing that TRPM7 and NLRP3 are potential pharmacological targets for the treatment of SE.

Additionally, TRPM7- mediated Ca^{2+} overload triggered neuronal death and subsequent pathological conditions [16, 17]. Here, we found that TRPM7 triggered pyroptosis via Zn^{2+}. Most Zn^{2+} exists in the Zn^{2+} -bound proteins, and free Zn^{2+} is mainly localized in the presynaptic vesicles of neurons [56]. Under pathological conditions, free Zn^{2+} is released from presynaptic terminals of neurons and enter postsynaptic neurons via multiple ion channels [57]. Zn^{2+} induces accumulation of toxic free radicals, leading to neuronal death [58]. We found that Zn^{2+} accumulated in the hippocampus of PILO-treated SE mice with TSQ staining, suggesting that Zn^{2+} might act as a core factor that contributes to the development of SE. Additionally, TRPM7 contributes to the accumulation of Zn^{2+} in mouse cortical neurons, and inhibiting TRPM7 with 2-APB or sh-RNA reduced Zn^{2+}-induced neuronal damage [59]. We also showed that chelating Zn^{2+} with TPEN suppressed the levels of these pyroptosis related factors, suggesting that TRPM7-mediated Zn^{2+} could be partially responsible for pyroptosis. Interestingly, treating TRPM7-overexpressed N2a cells with the Fe^{2+} chelator DFX and Cu^{2+} chelator TTM did not affect the levels of pyroptosis associated molecules, denying the possibility that pyroptosis could be triggered partially via TRPM7-mediated Fe^{2+} or Cu^{2+}. Therefore, we first establish that TRPM7-mediated Zn^{2+} contributes to pyroptosis in SE.

STAT3 is a latent transcription factor that mediates many important cellular functions including proliferation, differentiation, migration, apoptosis, and immunity [60–63]. After phosphorylation on residue Y705, p-STAT3 translocates to the nucleus to interact with specific regions, contributing to the transcription of target genes [64]. The levels of STAT3 and p-STAT3 protein as well as STAT3 phosphorylation (p-STAT3/STAT3) are increased in the hippocampus of PILO-treated animal models of epilepsy [41, 43]. We observed that the protein levels of STAT3 and p-STAT3/STAT3 were also enhanced in the SE model. Moreover, the protein levels of STAT3 and p-STAT3/STAT3 were further increased in TRPM7-overexpressed N2a cells, and this increase could be abolished by TPEN, while not be affected by DFX and TTM. These finding suggested that TRPM7-mediated Zn^{2+} promotes the expression and activation of STAT3 in SE. Meanwhile, STAT3 knockdown down-regulated the mRNA levels of TRPM7 and NLRP3 in PILO-treated N2a cells. P-STAT3 could be recruited to the promoter regions of *Trpm7* and *Nlrp3* in N2a cells. Moreover, inhibiting STAT3 phosphorylation with Stattic decreased the NLRP3 protein level in PILO-treated N2a cells. Therefore, p-STAT3 can translocate to the nucleus and interact directly with *Trpm7* and *Nlrp3* promoters to increase their transcriptions in SE.

Here, NS8593 alleviated neuronal damage and pyroptosis while reversing neuronal hyperexcitability in PILO-treated mice models of SE. Thus, the inhibition of TRPM7 could reverse neuronal damage, pyroptosis, and hyperexcitability in SE. However, NS8593 not only negatively modulates the TRPM7 channel, but also can affect small conductance Ca^{2+}-activated K^+ (SK), and the TRPM3 channel [33]. Going forward, more specific inhibitors of TRPM7 should be applied. SDUY-225 was a new compound designed according to the structure of NS8593, and the IC_{50} value of SDUY-225 was distantly lower than that of NS8593, indicative of higher potency. Our data indicated that SDUY-225 treatment was far superior to NS8593 in reversing neuronal damage, pyroptosis, and hyperexcitability in SE. Hence, the inhibition of TRPM7 by SDUY-225 is a promising strategy for SE treatment.

Conclusions

Based on our findings, we propose a simplified schematic model describing a novel mechanism by which TRPM7-induced pyroptosis in SE (Fig. 11). In models of epilepsy, the expression of STAT3 and p-STAT3 are up-regulated, p-STAT3 was translocated into nucleus acts as a

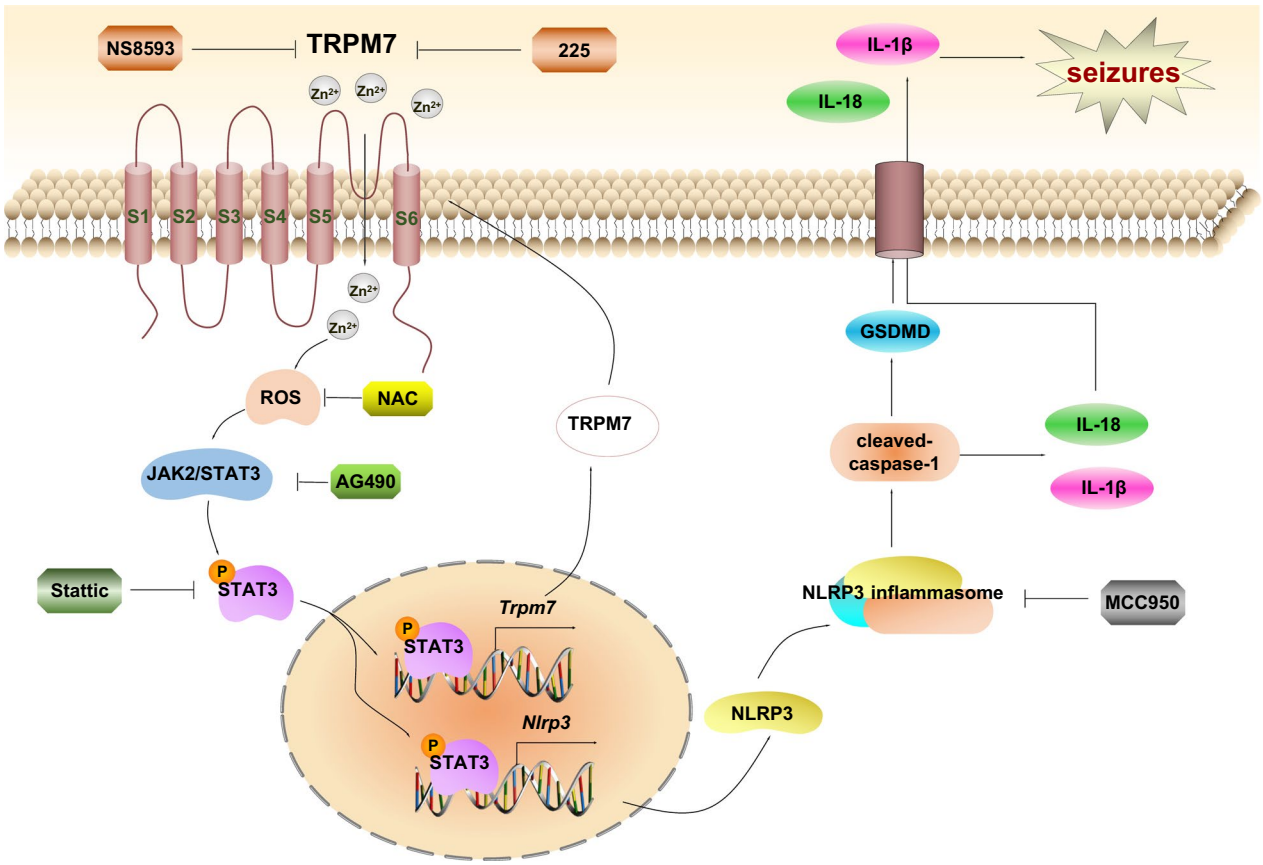

Fig. 11 A proposed schematic describes the mechanism of TRPM7-induced pyroptosis in SE. The up-regulated TRPM7 in SE cells increases the influx and accumulation of Zn^{2+}, which induces ROS generation to further induces the activation of JAK2/STAT3 pathway. Then p-STAT3 translocates to the nuclear to promote the transcription and expression of NLRP3 and TRPM7. The activation of NLRP3 inflammasome triggers caspase-1 activation, which cleaves and activates the IL-18 and IL-1β, and GSDMD. GSDMD-N terminal oligomerizes and form pores in plasma membrane where mature IL-1β and IL-18 are released. Inhibiting TRPM7 with NS8593, p-STAT3 inhibitor Stattic and NLRP3 inflammasome inhibitor MCC950 could reserve the hyperexcitability in SE models in vivo and in vitro

dual-target transcription factor that binds to the promoters of *Nlrp3* and *Trpm7* thereby resulting in the increased expression of NLRP3 and TRPM7. Furthermore, elevated TRPM7 protein levels promote increased influx of Zn^{2+}, forming a positive feedback loop of p-STAT3/TRPM7/Zn^{2+}/p-STAT3, and triggering pyroptosis associated factors which included NLRP3, caspase-1 p20, IL-1β, IL-18, and GSDMD. Additionally, SDUY-225, as well as NS8593 and MCC950 reduced hyperexcitability in SE models. We describe a detailed mechanism implicating TRPM7 in the regulation of pyroptosis, thereby providing new insights into possible therapeutic targets in SE. Overall, our study provides compelling evidence that exploring new TRPM7 inhibitor is a potent starting point for the treatment of various diseases via inhibition of pyroptosis.

Abbreviations

AD	Alzheimer disease
ALS	Amyotrophic lateral sclerosis
Aps	Spontaneous action potentials
CA1	Cornu ammonis 1
CA3	Cornu ammonis 3
CCK-8	Cell counting Kit-8 assay
ChIP	Chromatin immunoprecipitation assay
CKO	Conditional knockout
DCFH-DA	Fluorescent probe 2,7-Dichlorodi-hydrofluorescein diacetate
DEGs	Differentially expressed genes
DFX	Deferoxamine
DG	Dentate gyrus
EEG	Electroencephalogram recordings
ELISA	Enzyme-linked immunosorbent assay
GFAP	Glial fibrillary acidic protein
GSDMD	Gasdermin D
IC_{50}	The half maximal inhibitory concentration
LPS	Lipopolysaccharide
MMP	Mitochondrial membrane potential
N2a	The mouse neuroblastoma neuro-2a cells
NeuN	Neuronal nuclei
NLRP3	NOD-like receptor family pyrin domain containing 3
OCT	Optimum cutting temperature compound
PD	Parkinson's disease
PILO	Pilocarpine
p-STAT3	Phosphorylated signal transducer and activator of transcription 3
PTZ	Pentylenetetrazole

pY^{705}-STAT3	STAT3 Tyr705 phosphorylation
qRT-PCR	Real-time quantitative reverse transcription PCR
ROS	Reactive oxygen species
SE	Status epilepticus
siRNA	Small interfering RNA
STAT3	Signal transducer and activator of transcription 3
TLC	Thin-layer chromatography
TPEN	The membrane-permeable Zn^{2+} chelator
TRM	Tremor rat
TRPM7	Transient receptor potential melastatin 7
TRPM7-CKO	TRPM7 conditional knockout
TSQ	The N-(6-methoxy-8-quinolyl)-para-toluenesulfonamide
TTM	Tetrathiomolybdate
SK	Small conductance Ca^{2+}-activated K^{+}

Supplementary Information

The online version contains supplementary material available at https://doi.org/10.1186/s12974-024-03292-4.

Additional file1 (PDF 205 KB)

Additional file2 (PDF 544 KB)

Additional file3 (PDF 2404 KB)

Additional file4 (DOCX 18 KB)

Acknowledgements
We sincerely appreciate the participants for their generous donation of samples.

Author contributions
Participated in research design, FG, WDZ, WYW and ZYY; Conducted experiments, XT, YT, JHZ, RXS, HYL, MXL, YLM, JS, DYZ, CRS, JLW, XXX, TB, SS, AF, RP, NNZ, JJX and JJD; Wrote or contributed to the writing of the manuscript, FG, WDZ, CRS and ZYY.

Funding
This work was supported by the National Natural Science Foundation of China (82473906, 81971212), the Shenyang Young and Middle-aged Technological Innovation Talent Support Program (RC210268), and the Natural Science Foundation of Liaoning Province (2023-MS-153).

Availability of data and materials
All data generated or analyzed during this study are included in this published article and its supplementary information files.

Declarations

Ethical approval and consent to participate
All animal protocols were approved by the Institutional Animal Care and Use Committee of China Medical University (CMU2021474). The human study complied with the Declaration of Helsinki and the ethical principles of the National Institutes of Health and was approved by the Committee on Human Research of the First Affiliated Hospital of China Medical University (20211020).

Consent for publication
Not applicable.

Competing interests
The authors declare no competing interests.

Author details
[1]Department of Pharmacy, The Fourth Affiliated Hospital of China Medical University, Shenyang 110032, China. [2]Department of Pharmaceutical Toxicology, School of Pharmacy, China Medical University, Shenyang 110122, China. [3]Department of Radiology, Shengjing Hospital of China Medical University, Shenyang 110022, China. [4]Department of Neurobiology, Boston Children's Hospital, Boston, MA 02115, USA. [5]Department of Neurology, the First Hospital of China Medical University, Shenyang 110001, China. [6]Department of Molecular Neurochemistry, Medical University of Lodz, 92215 Lodz, Poland. [7]Center for Biomedical Research, The Queen's Medical Center, 1301 Punchbowl St, Honolulu, HI 96813, USA. [8]John A. Burns School of Medicine, University of Hawaii, 651 Ilalo St, Honolulu, HI 96813, USA. [9]University of Hawaii Cancer Center, University of Hawaii, 651 Ilalo St, Honolulu, HI 96813, USA. [10]Division of Medicinal Chemistry, School of Pharmaceutical Sciences, Shandong University, Shandong 250012, China. [11]Department of Physiology, Graduate School of Medical and Dental Sciences, Kagoshima University, Kagoshima 890-8544, Japan. [12]Human Aging Research Institute and School of Life Sciences, Nanchang University, Nanchang 330031, Jiangxi, China. [13]Jiangsu Province Key Laboratory of Anesthesiology, Xuzhou Medical University, Xuzhou 221002, China. [14]Department of Developmental Cell Biology, China Medical University, Shenyang 110122, China. [15]Department of Cell Biology, Key Laboratory of Cell Biology, Ministry of Public Health, Key Laboratory of Medical Cell Biology, Ministry of Education, School of Life Sciences, China Medical University, Shenyang 110122, China.

Received: 3 September 2024 Accepted: 11 November 2024
Published online: 01 December 2024

References

1. Shi J, Gao W, Shao F. Pyroptosis: Gasdermin-Mediated Programmed Necrotic Cell Death. Trends Biochem Sci. 2017;42:245–54.
2. Yu P, Zhang X, Liu N, Tang L, Peng C, Chen X. Pyroptosis: mechanisms and diseases. Signal Transduct Target Ther. 2021;6:128.
3. Moujalled D, Strasser A, Liddell JR. Molecular mechanisms of cell death in neurological diseases. Cell Death Differ. 2021;28:2029–44.
4. Thijs RD, Surges R, O'Brien TJ, Sander JW. Epilepsy in adults. Lancet. 2019;393:689–701.
5. Trinka E, Cock H, Hesdorffer D, Rossetti AO, Scheffer IE, Shinnar S, Shorvon S, Lowenstein DH. A definition and classification of status epilepticus–Report of the ILAE Task Force on Classification of Status Epilepticus. Epilepsia. 2015;56:1515–23.
6. Sombati S, Delorenzo RJ. Recurrent spontaneous seizure activity in hippocampal neuronal networks in culture. J Neurophysiol. 1995;73:1706–11.
7. Curia G, Longo D, Biagini G, Jones RS, Avoli M. The pilocarpine model of temporal lobe epilepsy. J Neurosci Methods. 2008;172:143–57.
8. Kalviainen R, Salmenpera T. Do recurrent seizures cause neuronal damage? A series of studies with MRI volumetry in adults with partial epilepsy. Prog Brain Res. 2002;135:279–95.
9. Fujikawa DG, Shinmei SS, Cai B. Seizure-induced neuronal necrosis: implications for programmed cell death mechanisms. Epilepsia. 2000;41(Suppl 6):S9-13.
10. Meng XF, Tan L, Tan MS, Jiang T, Tan CC, Li MM, Wang HF, Yu JT. Inhibition of the NLRP3 inflammasome provides neuroprotection in rats following amygdala kindling-induced status epilepticus. J Neuroinflammation. 2014;11:212.
11. Wang Z, Zhou L, An D, Xu W, Wu C, Sha S, Li Y, Zhu Y, Chen A, Du Y, et al. TRPV4-induced inflammatory response is involved in neuronal death in pilocarpine model of temporal lobe epilepsy in mice. Cell Death Dis. 2019;10:386.
12. Li X, Lin J, Hua Y, Gong J, Ding S, Du Y, Wang X, Zheng R, Xu H. Agmatine Alleviates Epileptic Seizures and Hippocampal Neuronal Damage by Inhibiting Gasdermin D-Mediated Pyroptosis. Front Pharmacol. 2021;12:627557.
13. Cristina de Brito Toscano E, Leandro Marciano Vieira E, Boni Rocha Dias B, Vidigal Caliari M, Paula Goncalves A, Varela Giannetti A, Mauricio Siqueira J, Kimie Suemoto C, Elaine Paraizo Leite R, Nitrini R, et al: NLRP3 and NLRP1 inflammasomes are up-regulated in patients with mesial temporal lobe epilepsy and may contribute to overexpression of caspase-1 and IL-beta in sclerotic hippocampi. *Brain Res* 2021, 1752:147230.
14. Kraft R, Harteneck C. The mammalian melastatin-related transient receptor potential cation channels: an overview. Pflugers Arch. 2005;451:204–11.
15. Huang Y, Fliegert R, Guse AH, Lu W, Du J. A structural overview of the ion channels of the TRPM family. Cell Calcium. 2020;85: 102111.

16. Aarts M, Iihara K, Wei WL, Xiong ZG, Arundine M, Cerwinski W, MacDonald JF, Tymianski M. A key role for TRPM7 channels in anoxic neuronal death. Cell. 2003;115:863–77.
17. Sun HS, Jackson MF, Martin LJ, Jansen K, Teves L, Cui H, Kiyonaka S, Mori Y, Jones M, Forder JP, et al. Suppression of hippocampal TRPM7 protein prevents delayed neuronal death in brain ischemia. Nat Neurosci. 2009;12:1300–7.
18. Hermosura MC, Garruto RM. TRPM7 and TRPM2-Candidate susceptibility genes for Western Pacific ALS and PD? Biochim Biophys Acta. 2007;1772:822–35.
19. Sun Y, Sukumaran P, Schaar A, Singh BB. TRPM7 and its role in neurodegenerative diseases. Channels (Austin). 2015;9:253–61.
20. Monteilh-Zoller MK, Hermosura MC, Nadler MJ, Scharenberg AM, Penner R, Fleig A. TRPM7 provides an ion channel mechanism for cellular entry of trace metal ions. J Gen Physiol. 2003;121:49–60.
21. Jeong JH, Lee SH, Kho AR, Hong DK, Kang DH, Kang BS, Park MK, Choi BY, Choi HC, Lim MS, Suh SW: The Transient Receptor Potential Melastatin 7 (TRPM7) Inhibitors Suppress Seizure-Induced Neuron Death by Inhibiting Zinc Neurotoxicity. *Int J Mol Sci* 2020, 21.
22. Gong L, Zhu T, Chen C, Xia N, Yao Y, Ding J, Xu P, Li S, Sun Z, Dong X, et al. Miconazole exerts disease-modifying effects during epilepsy by suppressing neuroinflammation via NF-kappaB pathway and iNOS production. Neurobiol Dis. 2022;172: 105823.
23. Noches V, Rivera C, Gonzalez MP, Merello G, Olivares-Costa M, Andres ME. Pilocarpine-induced seizures associate with modifications of LSD1/CoREST/HDAC1/2 epigenetic complex and repressive chromatin in mice hippocampus. Biochem Biophys Rep. 2021;25: 100889.
24. Guo F, Zhou PD, Gao QH, Gong J, Feng R, Xu XX, Liu SY, Hu HY, Zhao MM, Adam HC, et al. Low-Mg(2+) treatment increases sensitivity of voltage-gated Na(+) channels to Ca(2+)/calmodulin-mediated modulation in cultured hippocampal neurons. Am J Physiol Cell Physiol. 2015;308:C594-605.
25. Zhao G, Oztan A, Ye Y, Schwarz TL. Kinetochore Proteins Have a Post-Mitotic Function in Neurodevelopment. Dev Cell. 2019;48(873–882): e874.
26. Thompson CH, Hawkins NA, Kearney JA, George AL Jr. CaMKII modulates sodium current in neurons from epileptic Scn2a mutant mice. Proc Natl Acad Sci U S A. 2017;114:1696–701.
27. Sparks FT, Liao Z, Li W, Grosmark A, Soltesz I, Losonczy A. Hippocampal adult-born granule cells drive network activity in a mouse model of chronic temporal lobe epilepsy. Nat Commun. 2020;11:6138.
28. Miyamoto H, Tatsukawa T, Shimohata A, Yamagata T, Suzuki T, Amano K, Mazaki E, Raveau M, Ogiwara I, Oba-Asaka A, et al. Impaired cortico-striatal excitatory transmission triggers epilepsy. Nat Commun. 1917;2019:10.
29. Priel MR, Albuquerque EX. Short-term effects of pilocarpine on rat hippocampal neurons in culture. Epilepsia. 2002;43(Suppl 5):40–6.
30. Serikawa T, Ohno Y, Sasa M, Yamada J, Takaori S. A new model of petit mal epilepsy: spontaneous spike and wave discharges in tremor rats. Lab Anim. 1987;21:68–71.
31. Shi J, Zhao Y, Wang K, Shi X, Wang Y, Huang H, Zhuang Y, Cai T, Wang F, Shao F. Cleavage of GSDMD by inflammatory caspases determines pyroptotic cell death. Nature. 2015;526:660–5.
32. Abumaria N, Li W, Clarkson AN. Role of the chanzyme TRPM7 in the nervous system in health and disease. Cell Mol Life Sci. 2019;76:3301–10.
33. Chubanov V. Mederos y Schnitzler M, Meissner M, Schafer S, Abstiens K, Hofmann T, Gudermann T: Natural and synthetic modulators of SK (K(ca)2) potassium channels inhibit magnesium-dependent activity of the kinase-coupled cation channel TRPM7. Br J Pharmacol. 2012;166:1357–76.
34. Duan J, Li Z, Li J, Hulse RE, Santa-Cruz A, Valinsky WC, Abiria SA, Krapivinsky G, Zhang J, Clapham DE. Structure of the mammalian TRPM7, a magnesium channel required during embryonic development. Proc Natl Acad Sci U S A. 2018;115:E8201-e8210.
35. Sensi SL, Paoletti P, Bush AI, Sekler I. Zinc in the physiology and pathology of the CNS. Nat Rev Neurosci. 2009;10:780–91.
36. Li X, Yang W, Jiang LH. Alteration in Intracellular Zn(2+) Homeostasis as a Result of TRPM2 Channel Activation Contributes to ROS-Induced Hippocampal Neuronal Death. Front Mol Neurosci. 2017;10:414.
37. Radford RJ, Lippard SJ. Chelators for investigating zinc metalloneurochemistry. Curr Opin Chem Biol. 2013;17:129–36.
38. Smirnova J, Kabin E, Jarving I, Bragina O, Tougu V, Plitz T, Palumaa P: Copper(I)-binding properties of de-coppering drugs for the treatment of Wilson disease. alpha-Lipoic acid as a potential anti-copper agent. *Sci Rep* 2018, 8:1463.
39. Kontoghiorghe CN, Kontoghiorghes GJ. Efficacy and safety of iron-chelation therapy with deferoxamine, deferiprone, and deferasirox for the treatment of iron-loaded patients with non-transfusion-dependent thalassemia syndromes. Drug Des Devel Ther. 2016;10:465–81.
40. Zhong Z, Wen Z, Darnell JE Jr. Stat3: a STAT family member activated by tyrosine phosphorylation in response to epidermal growth factor and interleukin-6. Science. 1994;264:95–8.
41. Grabenstatter HL, Del Angel YC, Carlsen J, Wempe MF, White AM, Cogswell M, Russek SJ, Brooks-Kayal AR. The effect of STAT3 inhibition on status epilepticus and subsequent spontaneous seizures in the pilocarpine model of acquired epilepsy. Neurobiol Dis. 2014;62:73–85.
42. Jiang Q, Tang G, Zhong XM, Ding DR, Wang H, Li JN. Role of Stat3 in NLRP3/caspase-1-mediated hippocampal neuronal pyroptosis in epileptic mice. Synapse. 2021;75: e22221.
43. Xu Z, Xue T, Zhang Z, Wang X, Xu P, Zhang J, Lei X, Li Y, Xie Y, Wang L, et al. Role of signal transducer and activator of transcription-3 in up-regulation of GFAP after epilepsy. Neurochem Res. 2011;36:2208–15.
44. Li X, Du X, Ni J: Zn(2+) Aggravates Tau Aggregation and Neurotoxicity. *Int J Mol Sci* 2019, 20.
45. Sun SY. N-acetylcysteine, reactive oxygen species and beyond. Cancer Biol Ther. 2010;9:109–10.
46. De Vos J, Jourdan M, Tarte K, Jasmin C, Klein B. JAK2 tyrosine kinase inhibitor tyrphostin AG490 downregulates the mitogen-activated protein kinase (MAPK) and signal transducer and activator of transcription (STAT) pathways and induces apoptosis in myeloma cells. Br J Haematol. 2000;109:823–8.
47. Pekny M, Nilsson M. Astrocyte activation and reactive gliosis. Glia. 2005;50:427–34.
48. Nagao T, Alonso A, Avoli M. Epileptiform activity induced by pilocarpine in the rat hippocampal-entorhinal slice preparation. Neuroscience. 1996;72:399–408.
49. Nadler MJ, Hermosura MC, Inabe K, Perraud AL, Zhu Q, Stokes AJ, Kurosaki T, Kinet JP, Penner R, Scharenberg AM, Fleig A: LTRPC7 is a Mg.ATP-regulated divalent cation channel required for cell viability. *Nature* 2001, 411:590–595.
50. Rong S, Wan D, Fan Y, Liu S, Sun K, Huo J, Zhang P, Li X, Xie X, Wang F, Sun T. Amentoflavone Affects Epileptogenesis and Exerts Neuroprotective Effects by Inhibiting NLRP3 Inflammasome. Front Pharmacol. 2019;10:856.
51. Xia S, Yang P, Li F, Yu Q, Kuang W, Zhu Y, Lu J, Wu H, Li L, Huang H. Chaihu-Longgu-Muli Decoction exerts an antiepileptic effect in rats by improving pyroptosis in hippocampal neurons. J Ethnopharmacol. 2021;270: 113794.
52. Shi R, Fu Y, Zhao D, Boczek T, Wang W, Guo F. Cell death modulation by transient receptor potential melastatin channels TRPM2 and TRPM7 and their underlying molecular mechanisms. Biochem Pharmacol. 2021;190: 114664.
53. Decker AR, McNeill MS, Lambert AM, Overton JD, Chen YC, Lorca RA, Johnson NA, Brockerhoff SE, Mohapatra DP, MacArthur H, et al. Abnormal differentiation of dopaminergic neurons in zebrafish trpm7 mutant larvae impairs development of the motor pattern. Dev Biol. 2014;386:428–39.
54. Landman N, Jeong SY, Shin SY, Voronov SV, Serban G, Kang MS, Park MK, Di Paolo G, Chung S, Kim TW. Presenilin mutations linked to familial Alzheimer's disease cause an imbalance in phosphatidylinositol 4,5-bisphosphate metabolism. Proc Natl Acad Sci U S A. 2006;103:19524–9.
55. Zhang H, Yu S, Xia L, Peng X, Wang S, Yao B. NLRP3 Inflammasome Activation Enhances ADK Expression to Accelerate Epilepsy in Mice. Neurochem Res. 2022;47:713–22.
56. Franco-Pons N, Casanovas-Aguilar C, Arroyo S, Rumia J, Perez-Clausell J, Danscher G. Zinc-rich synaptic boutons in human temporal cortex biopsies. Neuroscience. 2000;98:429–35.
57. Frederickson CJ, Suh SW, Silva D, Frederickson CJ, Thompson RB. Importance of zinc in the central nervous system: the zinc-containing neuron. J Nutr. 2000;130:1471S-1483S.
58. Kim EY, Koh JY, Kim YH, Sohn S, Joe E, Gwag BJ. Zn2+ entry produces oxidative neuronal necrosis in cortical cell cultures. Eur J Neurosci. 1999;11:327–34.

59. Inoue K, Branigan D, Xiong ZG. Zinc-induced neurotoxicity mediated by transient receptor potential melastatin 7 channels. J Biol Chem. 2010;285:7430–9.
60. You L, Wang Z, Li H, Shou J, Jing Z, Xie J, Sui X, Pan H, Han W. The role of STAT3 in autophagy. Autophagy. 2015;11:729–39.
61. Hillmer EJ, Zhang H, Li HS, Watowich SS. STAT3 signaling in immunity. Cytokine Growth Factor Rev. 2016;31:1–15.
62. Wang B, Liu T, Wu JC, Luo SZ, Chen R, Lu LG, Xu MY. STAT3 aggravates TGF-beta1-induced hepatic epithelial-to-mesenchymal transition and migration. Biomed Pharmacother. 2018;98:214–21.
63. Damasceno LEA, Prado DS, Veras FP, Fonseca MM, Toller-Kawahisa JE, Rosa MH, Publio GA, Martins TV, Ramalho FS, Waisman A, et al: PKM2 promotes Th17 cell differentiation and autoimmune inflammation by fine-tuning STAT3 activation. *J Exp Med* 2020, 217.
64. Bromberg J, Darnell JE Jr. The role of STATs in transcriptional control and their impact on cellular function. Oncogene. 2000;19:2468–73.

Publisher's Note